Local Polynomial Fourier Transform: A Review on Recent Developments and Applications

Xiumei Li, Guoan Bi, Srdjan Stanković, Abdelhak M. Zoubir

Abstract— **The local polynomial Fourier transform (LPFT), as a high-order generalization of the short-time Fourier transform (STFT), has been developed and used for many different applications in recent years. This paper attempts to review previous research work on the following issues of the LPFT. Firstly, the definition and properties of the LPFT and its relationships with other transforms are reviewed. The LPFT for multicomponent signal is then presented. The polynomial time frequency transform (PTFT), which is the maximum likelihood estimator to estimate the parameters in the LPFT, as well as its properties and fast algorithms, are discussed. By comparing with the Fourier transform (FT), the STFT and the Wigner-Ville distribution (WVD), the LPFT has its superiority in obtaining improved SNRs, which can be supported by theoretical analysis and computer simulations. Furthermore, the reassignment method is combined with the LPFT and the robust LPFT to improve the concentration of the signal representation in the time-frequency domain. Performance obtained by using various LPP-related methods are compared for signals in different noise environments, such as the additive white Gaussian noise (AGWN), impulsive noise, and the mixture of AGWN and impulsive noise.**

I. Introduction

In many practical applications, such as radar, sonar, and communications, the signals under consideration are usually time-varying, that is, their frequencies are varying with time. According to the Weierstrass approximation theorem [1], the phase of an arbitrary time-varying signal can be well approximated by a polynomial of sufficient order. This kind of time-varying signals with polynomial phase, also known as the polynomial-phase signals (PPSs), is of significant importance. The PPSs have been reported to be used in many different areas, such as biomedical engineering [10], image processing [11], image and audio watermarking [12], motion estimation in video sequence [13], [14], communications [15], [16], [17], sonar [18] and radar applications [2], [19]. The general form of the $(r+1)$th-order PPS is expressed as

$$x(n) = A(n)e^{j2\pi\sum_{m=0}^{r} a_m n^m} + \eta(n), \qquad (1)$$

$$n = 0, 1, ..., N-1,$$

where the amplitude $A(n)$ is a constant or a real-valued stationary Gaussian process, $a_m, 0 \le m \le r$ are the coefficients associated with the polynomial phase, and $\eta(n)$ is white Gaussian noise.

For this kind of time-varying signals, it is far more useful to characterize them with the time-frequency representations (TFRs), which describe how the frequency content of a signal evolves over the time and help us to obtain more detailed information of the time-varying signals. There exist many different TFRs, and they generally falling into two categories, which are linear TFRs and nonlinear TFRs [3], [20], [22]. Linear TFRs mainly include the STFT and the wavelet transform. Nonlinear TFRs include the WVD, the ambiguity function (AF), smoothed versions of the WVD, and the Cohen's class. Some of the widely used transforms are expressed as follows:

- STFT.

$$\mathrm{STFT}(x;t,\omega) = \int_{-\infty}^{\infty} x(t+\tau)h^*(\tau)e^{-j\omega\tau}d\tau, \quad (2)$$

where $h(\tau)$ is the window function of finite sequence length. For simplicity in the rest of the

Signal Processing, Special Issue on Fourier Related Transforms for Non-Stationary Signals, Vol. 91, No. 6. June 2011.

paper, the integral without limits implies that the integration is from $-\infty$ to ∞.

- WVD.

$$\mathrm{WVD}(x;t,\omega) = \\ = \int x(t+\tau/2)x^*(t-\tau/2)e^{-j\omega\tau}d\tau, \quad (3)$$

which is obtained by performing the FT with respect to the variable τ.

- AF.

$$\mathrm{AF}(x;\theta,\tau) = \int x(t+\frac{\tau}{2})x^*(t-\frac{\tau}{2})e^{j\theta t}dt. \quad (4)$$

which is obtained by performing the Fourier transform with respect to the variable t.

Each TFR has its individual advantages and disadvantages. For example, the linear STFT is simple to implement and free from the cross terms for multicomponent signals, but it only provides low resolution for time-varying signals. In contrast, the WVD provides high resolution but contains cross terms for multicomponent signals. The local polynomial Fourier transform (LPFT), which is a generalized form of the STFT, was presented recently [22]. Since it uses extra parameters to approximate the instantaneous frequency (IF) characteristic of the PPSs, the LPFT can provide much better concentration and resolution than the STFT. Moreover, due to its linearity, the LPFT is free from the cross terms that exist in the WVD. The LPFT has received considerable attention in the past years, and has been used in a variety of applications, such as instantaneous frequency (IF) estimation [22], [23], radar imaging [24], [25], interference suppression in communications [26], [27], and motion parameter estimation in video sequences [14].

In this paper, we will first review the previous research on the LPFT such as its definition, properties and relationships with other transforms in Section II. The LPFT for multicomponent signals is then presented in Section III. In Section IV, the PTFT as well as its properties is introduced and its fast algorithms are reviewed. Section V gives the theoretical SNR analysis of the LPFT, and shows that the LPFT can provide higher SNR than the FT, the STFT and the WVD. In Section VI, the reassignment method is extended to the LPFT to improve the concentration of the signals in the time-frequency domain. The reassignment method is also combined with the robust methods to process signals in impulsive noise. Furthermore, performances achieved by using various LPP-related methods are compared for signals in different noise environments, in terms of readability, computation complexity, distribution concentration, and mean squared error (MSE) of IF estimation. Application examples of the LPFT are reviewed in Section VII and potential applications of the LPFT are also discussed. Finally, conclusions are drawn in Section VIII.

II. Definition, properties, and relationships with other transforms

In this section, we will review the definition and properties of the LPFT, and its relationships with the STFT, the WVD, the AF and the fractional Fourier transform (FrFT).

A. Definition and properties

To approximate the local polynomial function, the LPFT introduces polynomial parameters including the first-order derivative and other higher-order derivatives of the IF of the analyzed signal. The form of the LPFT is as follows [22]:

$$\mathrm{LPFT}(x;t,\varpi) = \mathrm{LPFT}(x;t,\omega,\omega_1\cdots\omega_{M-1}) \\ = \int x(t+\tau)h(\tau)e^{-j\theta(\tau,\varpi)}d\tau, \quad (5)$$

where

$$\theta(\tau,\varpi) = \omega\tau + \omega_1\tau^2/2 + \cdots + \omega_{M-1}\tau^M/M!,$$

$$\varpi = (\omega,\omega_1,\cdots,\omega_{M-1}),$$

and M is the order of the LPFT. The local polynomial periodogram (LPP) is defined as

$$\mathrm{LPP}(x;t,\varpi) = |\mathrm{LPFT}(x;t,\varpi)|^2. \quad (6)$$

For the LPFT, the corresponding form of Parseval's theorem can be written as [28]

$$\frac{1}{2\pi}\int |\mathrm{LPFT}(x;t,\varpi)|^2 d\omega =$$

$$= \int |x(t+\tau)h(\tau)|^2 d\tau, \tag{7}$$

which indicates that the LPFT can be interpreted as a time-frequency energy distribution over the $t - \boldsymbol{\omega}^0(t)$ space, where $\boldsymbol{\omega}^0(t) = [\Omega(t), \Omega^{(1)}(t), \cdots, \Omega^{(M-1)}(t)]^T$ is a vector of the true values of the IF $\Omega(t)$ and its derivatives. The energy concentration of $\mathrm{LPFT}(t, \boldsymbol{\omega})$ in $\boldsymbol{\omega}^0(t)$ for the time instant t is illustrated in [22], [23]. This concentration motivates the use of the LPFT as an IF estimator, and asymptotic covariance matrix and bias of the estimates are studied in [22], [23]. It is shown that the window bandwidth controls the tradeoff of bias and variance. Therefore, the estimation accuracy depends on the window bandwidth and the optimization of bandwidth can greatly improve the accuracy. Meanwhile increasing the order M can also improve the accuracy in a useful way given the relevant choice of the bandwidth [23]. A data-driven approach based on the intersection of confidence intervals (ICI) was proposed in [29] to solve the problem of bandwidth selection and a varying adaptive window size can be selected to optimize the local accuracy of the estimation. Asymptotic variance and bias analysis for the discrete-time LPFT is presented in [23], and the asymptotic behavior includes the long-time asymptotic with long window length, and the short-time asymptotic with short window length. The LPFTs with the symmetric window and nonsymmetric window are discussed in [30], [31]. For the LPFT with the symmetric window, the estimators with $M = 1$ and 2 achieve the equivalent accuracy of the IF estimation, and increasing the order from $M = 2$ to 3 results in an increase of the variance and a decrease of the bias. While for the LPFT with the nonsymmetric window, increasing the order M always results in an increase of the variance of the IF estimation and a decrease of the bias. The LPFT estimates with the symmetric window have a great advantage compared with those with the nonsymmetric window. It should be noted that when nonsymmetric rectangular window is used, the LPFT estimator coincides with the maximum likelihood estimator [30], [31].

The principal difference between the LPFT and the quadratic and high-order TFRs has been discussed in [22]. The LPFT is linear with respect to the signal and uses the polynomial function, $\theta(\tau, \varpi)$, in the complex exponent (or the transform kernel). On the other hand, quadratic or higher degree polynomials of the signal are used in the definition of the quadratic or high-order TFRs, with the exponential function $e^{-j\omega\tau}$, wherein the argument of the exponent is linear with respect to variable τ.

Due to its linearity, the LPFT can be inversed to reconstruct the original signal by integrating the LPFT over ω, that is

$$x(t) = \frac{1}{2\pi h(0)} \int \mathrm{LPFT}(x; t, \varpi) d\omega. \tag{8}$$

B. Relationships with other transforms

The LPFT is related with many other transforms, such as the STFT, the WVD, the AF and the FrFT. The relationships will be investigated as follows.

B.1 STFT

In (5) when $M = 1$, the LPFT becomes the STFT. Therefore the LPFT is a generalization of the STFT.

B.2 WVD

It has been reported in [4] that the STFT is related to the WVD by:

$$|\mathrm{STFT}(s; t, \omega)|^2 = \int\int \mathrm{WVD}(s; \tau, \theta)$$

$$\times \mathrm{WVD}(h; t - \tau, \omega - \theta) d\tau d\theta \tag{9}$$

where $\mathrm{WVD}(s; t, \omega)$ and $\mathrm{WVD}(h; t, \omega)$ denote the WVDs of the analyzed signal $s(t)$ and the window function $h(t)$, respectively.

Similarly, the relationship of the LPFT and the WVD has been investigated in [32]:

$$|\mathrm{LPFT}(s; t, \omega)|^2 = \int\int \mathrm{WVD}(h; \tau, \theta)$$

$$\times \mathrm{WVD}(s; t - \tau, \omega - \omega_1 \tau - \theta) d\tau d\theta. \tag{10}$$

B.3 AF

The relationship between the STFT and the AF was reported as [33],

$$|\mathrm{STFT}(s;t,\omega)|^2 = \int\int \mathrm{AF}(s;\theta,\tau)$$

$$\times \mathrm{AF}(h;\theta,\tau)e^{-j(\theta t+\omega\tau)}d\tau d\theta. \quad (11)$$

Following the similar procedure, the relationship between the LPFT and the AF can be expressed as:

$$|\mathrm{LPFT}(s;t,\omega)|^2 = \int\int \mathrm{AF}(s;\tau,\theta-\omega_1\tau)$$

$$\times \mathrm{AF}(h;\tau,\theta)e^{-j(\theta t+\omega\tau-\omega_1 t\tau)}d\tau d\theta \quad (12)$$

B.4 FrFT

It was shown in [34] that for a linear frequency modulated (LFM) signal $s(t) = Ae^{j(a_1 t+\frac{b_1}{2}t^2)}$ the corresponding second-order LPFT is

$$|\mathrm{LPFT}(s;t,\omega)| = A\sqrt{\frac{2\pi}{|\omega_1-b_1|}}$$

$$\times \exp\left\{j\frac{(\omega-a_1-b_1 t)^2}{4(\omega_1-b_1)}\right\} * H(\omega), \quad (13)$$

where $*$ is the convolution in the frequency domain and $H(\omega)$ is the Fourier transform of the window function $h(t)$. Therefore the second-order LPFT is concentrated along the IF of the LFM signal, $\omega = a_1 + b_1 t$, for $\omega_1 = b_1$.

The FrFT, a generalization of the FT, is another method that can concentrate LFM signals. Its definition is expressed as [5]

$$\mathrm{F}_\alpha(u) =$$

$$= \begin{cases} \sqrt{\frac{1-j\cot\alpha}{2\pi}}e^{j(u^2/2)\cot\alpha} & \alpha \neq n\pi, \\ \times \int x(t)e^{j(t^2/2)\cot\alpha - jut\csc\alpha}dt, & \\ s(t), & \alpha = 2n\pi, \\ s(-t), & \alpha = (2n+1)\pi. \end{cases} \quad (14)$$

The FT is a special case of the FrFT with the rotation angle $\alpha = \frac{\pi}{2}$.

For $M = 2, \omega = u\csc\alpha$ and $\omega_1 = \cot\alpha$ in (5), the FrFT can be expressed in terms of the second-order LPFT as

$$F_\alpha(u) = \sqrt{\frac{1-j\cot\alpha}{2\pi}}e^{j(u^2/2)\cot\alpha}$$

$$\times \mathrm{LPFT}(s;t,\omega,\omega_1), \quad (15)$$

therefore the LPFT provides a broad generalization of the FrFT [21].

III. The LPFT for multicomponent signals

Multicomponent PPSs are very common in a variety of applications, such as radar and mobile communications [9], [37], [38]. To process the multicomponent signals, two LPFT methods are presented as follows.

A. Adaptive LPFT

The second-order LPFT with point-wise chirp rate parameter estimation was proposed as [24], [34]

$$\mathrm{LPFT}_{\alpha(t)}(x;t,\omega) =$$

$$= \int x(t+\tau)h^*(\tau)e^{-j\alpha(t)\tau^2/2}e^{-j\omega\tau}d\tau, \quad (16)$$

where $\alpha(t)$ is time-varying chirp parameters, which can be estimated by

$$\hat{\alpha}(t) = \arg\max_{\alpha\in\Lambda} H(\alpha,t), \quad (17)$$

where Λ is a set of values of considered chirp rate parameters, and $H(\alpha,t)$ is the concentration measure discussed in [35][36] which is defined as

$$H(\alpha,t) = \frac{\int |\mathrm{LPFT}_\alpha(t,\omega)|^2 d\omega}{(\int |\mathrm{LPFT}_\alpha(t,\omega)|\, d\omega)^{3/2}}. \quad (18)$$

This particular concentration measure can achieve very sharp maximum for α close to the second derivative of the signal phase [35].

For multicomponent signals, the adaptive LPFT was proposed in [34] with the weighted coefficients $g(\alpha,t)$ as

$$\mathrm{ALPFT}(t,\omega) = \sum_{\alpha\in\Lambda} g(\alpha,t)\mathrm{LPFT}_\alpha(t,\omega). \quad (19)$$

The weighted coefficients are selected according to the considered signal type. If a signal has numerous components but with similar chirp rates, then it is appropriate to set $g(\hat{\alpha}, t) = 1$ to ensure that all components can be concentrated reasonably, where $\hat{\alpha}(t)$ is the element from Λ producing the highest concentration in the considered instant (17) and $g(\alpha, t) = 0$ for $\alpha \neq \hat{\alpha}(t)$. For signals with numerous components but with several different chirp rates, the following steps can be used [34]:

- set $H^{(0)}(\alpha, t) = H(\alpha, t)$, $i = 0$;
- determine $\hat{\alpha}^{(i)}(t) = \arg\max_{\alpha} H^{(i)}(\alpha, t)$, $i = i + 1$;
- set $g(\hat{\alpha}^{(i)}(t), t) = 1$;
- set $\hat{H}^{(i)}(\alpha, t) = \hat{H}^{(i-1)}(\alpha, t)$ for $\alpha \notin [\hat{\alpha}^{(i)} - \Delta, \hat{\alpha}^{(i)} + \Delta]$, $\hat{H}^{(i)}(\alpha, t) = 0$ elsewhere.

These steps should be repeated for each chirp rate producing a high concentration measure, and the procedure can be ended when there are no more α-producing high values of $\hat{H}^{(i)}(\alpha, t)$.

B. Modified LPFT

For signals with multiple components, another efficient method known as the modified LPFT (MLPFT) was introduced in [39] for signals containing p component with sets of parameters $L(t) : l_i(t); 1 \leq i \leq p$ and window lengths $Q : Q_i; 1 \leq i \leq p$ as

$$\text{MLPFT}_p(t, \omega) = \int x(t + \tau) e^{-j\omega\tau \Sigma_{i=1}^{p} h_i(\tau)} \times e^{-j\Sigma_{m=2}^{M} l_{i,m-1}(t)(\tau^m/m!)} d\tau. \quad (20)$$

The parameter sets $L(t) : l_i(t); 1 \leq i \leq p$ can be estimated by using the maximum likelihood estimator, the PTFT, which will be introduced in Section IV. For the window length, it is initially selected to be small enough to provide acceptable accuracy of the approximation and the actual length of the window can be increased according to the properties of consecutive signal segments. More details on the application of the LPFT can be found in [39].

It is shown that for multicomponent signals, the cross terms using the LPFT have much smaller magnitudes compared with that of the autoterm [39]. The MLPFT generally has fewer cross terms than the bilinear transforms and can be approximately viewed as the sum of the LPFT of each component. The MLPFT is computed through the following steps:

- use a window function to divide the signal into a number of segments, and model each segment as an Mth-order PPS;
- estimate the phase parameters of each segment using the PTFT;
- compute LPFT with the estimated parameters and selected window length.

The length of overlap between two consecutive segments controls the computation load as well as the smoothness of the spectrum. It has been shown in [39] that the LPFT with no overlap can still yield satisfactory performance if the window length is small enough. In this way, the computational complexity can be greatly reduced. Furthermore, since the computation complexity of the LPFT increases with the order of the PPS, processing higher-order PPSs with lower order LPFT is another way to reduce the computational complexity. It should be noted that for higher-order PPSs, the second-order LPFT can employ a small window length to ensure that each segment within the window can be assumed to be a chirp signal. In this way, the second-order LPFT, which is particularly suitable to process the LFM signals, can also be used to process higher-order signals with time-varying frequencies, which has been shown in [39]. This arrangement may have problems of unsmoothness of the frequency components when consecutive segments are connected. Under this circumstance, the length of overlap between the adjacent segments should be increased to minimize the unsmoothness [39]. Therefore we focus on the second-order LPFT in this paper unless otherwise indicated.

IV. PTFT and its fast algorithms

As stated in Section III, the polynomial parameters can be estimated by using the PTFT [40], [41], which is the maximum likelihood estimator.The PTFT is a transform which converts a one-dimensional input signal into a multidimensional output from which the poly-

nomial coefficients are estimated. In this section, the PTFT and its properties will be introduced, and followed by the review on its fast algorithms.

A. PTFT and its properties

To estimate the parameters of the PPSs defined in (1), the $(r+1)$th-order PTFT is defined as [40], [41]

$$\mathrm{PTFT}(k_0,k_1,\cdots,k_r)=$$

$$=\sum_{n=0}^{N_0-1}x(n)W_{N_0}^{k_0n}W_{N_1}^{k_1n^2}\cdots W_{N_r}^{k_rn^{r+1}},\quad(21)$$

where $W_N=e^{-j2\pi/N}$, $x(n)$ is the one-dimensional (1-D) input sequence of N_0 points, $0\le k_i\le N_i-1$, for $i=0,1,...,r$, and N_i is the size of the ith dimension of $\mathrm{PTFT}(k_0,k_1,\cdots,k_r)$. For simplicity of presentation, a demodulated sequence is defined as $y^{(d)}(n)=y(n)W_{N_1}^{k_1n^2}\cdots W_{N_r}^{k_rn^{r+1}}$, then (21) can be expressed as

$$\mathrm{PTFT}(k_0,k_1,\cdots,k_r)=\sum_{n=0}^{N_0-1}y^{(d)}(n)W_{N_0}^{k_0n},\quad(22)$$

which means that the PTFT of $y(n)$ is equivalent to the discrete Fourier transform (DFT) of $y^{(d)}(n)$. Due to the property of DFT, sharp peaks appear in the PTFT if there exist sinusoidal signals in $y^{(d)}(n)$. This occurs when integer k_i for $i=1,\cdots,r$ take values satisfying $k_i/N_i\approx a_{i+1}$. Since the parameters $a_1,a_2,\cdots,a_M$ are estimated according to the defined grids, the performance of PTFT is influenced by the quantization errors δ_i, i.e., $\delta_i=a_{i+1}-k_i/N_i$, which can be controlled by the dimension size N_i. The frequency deviation due to the quantization errors δ_i is assumed to be much smaller than the frequency of the sinusoidal component, which can be expressed as [40]

$$\left|\sum_{i=1}^{M-1}n^i\delta_i\right|\le\left|\sum_{i=1}^{M-1}n^i/(2N_i)\right|\ll|a_1|\le0.5,\quad(23)$$
$$n=0,\cdots,N_0-1,$$

since the maximum quantization error δ_i along the ith dimension is $1/(2N_i)$. Otherwise the peak may not be easily identified due to the quantization errors. Therefore we have

$$\sum_{i=1}^{M-1}\frac{N_0^i}{N_i}\ll1,\quad(24)$$

which means that for $1\le i\le M-1$, $N_i\gg N_0^i$ is required to achieve a satisfactory accuracy for parameter estimation.

When the above constraint is satisfied the PTFT of a multicomponent PPS exhibits the same number of peaks as that of components in the PPS. From the location coordinates of the peaks, the parameters of the PPS can be estimated [40], [41], [86].

In fast algorithms for the PTFT, its symmetric property is usually used to reduce the computational complexity of the PTFT. The symmetric property of the PTFT can be described as [42]

$$\mathrm{PTFT}(k_0,k_1+\alpha_1\frac{N_1}{2},...,k_r+\alpha_r\frac{N_r}{2})=$$

$$=\begin{cases}\mathrm{PTFT}(k_0,k_1,...,k_r) & \text{if } \sum_{i=1}^{r}\alpha_i \text{ is even}\\ \mathrm{PTFT}(k_0+\frac{N_0}{2},k_1,...,k_r) & \text{if } \sum_{i=1}^{r}\alpha_i \text{ is odd}\end{cases}\quad(25)$$

where $0\le k_0\le N_0-1$, $0\le k_i\le N_i/2-1$, and $\alpha_i=0$ or 1 for $i=1,2,...,r$. This symmetric property indicates that the computation for those PTFT points with indexes $k_i=N_i/2,...,N_i-1$ is not necessary since they can be replaced by those with indexes $k_i=0,...,N_i/2-1$. For an $(r+1)$th-order PTFT, this property means that the space for each k_i can be reduced by one half. Thus, the entire PTFT computation space is reduced by 2^r times. With the symmetric property, for example, the third-order PTFT can be expressed as

$$\mathrm{PTFT}(k_0,k_1+\frac{N_1}{2},k_2+\frac{N_2}{2})=\mathrm{PTFT}(k_0,k_1,k_2)$$
$$\mathrm{PTFT}(k_0,k_1+\frac{N_1}{2},k_2)=\mathrm{PTFT}(k_0+\frac{N_0}{2},k_1,k_2)$$
$$\mathrm{PTFT}(k_0,k_1,k_2+\frac{N_2}{2})=\mathrm{PTFT}(k_0+\frac{N_0}{2},k_1,k_2)\quad(26)$$

where $k_i = 0, ..., N_i/2 - 1$. It can be verified that the total number of PTFT outputs is $(N_0 N_1 N_2)/4$ instead of $N_0 N_1 N_2$.

For real-valued sequence, the Hermitian property of the PTFT is defined as [43]

$$\mathrm{PTFT}(N_0 - k_0, ..., N_r - k_r) =$$

$$= \mathrm{PTFT}^*(k_0, ..., k_r). \tag{27}$$

This property indicates that for an $(r+1)$th-order PTFT, it is not necessary to calculate these transform points with $k_i = \lceil N_i/2 \rceil, ..., N_i - 1$, where $0 \le i \le r$, because they can be obtained from those with indexes $k_i = 1, ..., \lfloor N_i/2 \rfloor$. Thus, the number of transform outputs to be calculated is decreased from $\prod_{i=0}^{r} N_i$ to $(\lfloor N_i/2 \rfloor + 1) \prod_{j=0, j\neq i}^{r} N_j$, where $\lfloor x \rfloor$ returns an integer smaller than or equal to x and $\lceil x \rceil$ returns an integer larger than or equal to x.

For real-valued sequence the symmetric property of the PTFT also exists, and by applying the Hermitian property to the symmetric property, the following property can be achieved

$$\mathrm{PTFT}(N_0 - k_0, \beta_1 N_1 - k_1, \beta_r N_r - k_r) =$$

$$= \begin{cases} \mathrm{PTFT}^*(k_0, k_1, ..., k_r) & \text{if } \sum_{i=1}^{r} \beta_i \text{ is integer} \\ \mathrm{PTFT}^*(k_0 + \frac{N_0}{2}, k_1, ..., k_r) & \text{otherwise} \end{cases} \tag{28}$$

where $0 \le k_0 \le N_0 - 1$, $0 \le k_i \le N_i/2 - 1$ for $i = 1, ..., r-1$, $0 \le k_r \le \lfloor N_i/4 \rfloor$, and $\beta = 1$ or $1/2$ for $i = 1, ...r$. With this property, the range of k_i can be further reduced by roughly one-half. By using the symmetric and Hermitian properties, the total number of transform outputs to be calculated can be reduced to $N_0(\prod_{i=1}^{r-1} N_i)(\lfloor N_r/4 \rfloor + 1)/2^{r-1}$, [43].

B. Fast Algorithms of the PTFT

The LPFT is computationally demanding because it is based on the PTFT estimation which involves calculating a multidimensional function and finding the maximum of the multidimensional function. Assuming the input sequence length N is a power of two, with the help of the fast Fourier transform (FFT), the $(r+1)$th-order PTFT can reduce its complexity from the order of $(\prod_{i=1}^{r} N_i)N^2$ to $(\prod_{i=1}^{r} N_i)N \log_2 N$, which is still difficult to support even with high speed processors. Luckily, various fast algorithms [40], [42]-[48] have been proposed to further reduce the computational complexity of the PTFT, which will be reviewed as follows.

To achieve a better computational efficiency, the fast quadratic phase transform [40] was proposed for the second-order PTFT. Compared with the FFT version of the PTFT, the fast quadratic phase transform can reduce the computational complexity by a factor $\log_2 N$. This work was extended to the third-order PTFT by exploiting the symmetric properties of the PTFT [44]. Although the DFT and PTFT differ in several ways, it shows that the PTFT can be decomposed into computation stages in a way similar to that for the FFT. Therefore, the total computational complexity can be significantly reduced. For example, the multiplicative complexity is reduced by a factor of $1.6\log_2 N_0$ compared with the method which directly uses the FFT. Furthermore, the fast algorithm was generalized to support an arbitrary order PTFT in [43], based on the decimation-in-time (DIT) decomposition technique, to reduce the overall computational complexity. For example, the numbers of complex multiplications and additions are reduced by a factor of $2^r \log_2 N$ for the $(r+1)$th-order PTFT of length-N input sequence, compared with the algorithm that directly uses the 1D FFTs.

However, further reduction on computational complexity was still possible since some properties of the PTFT are not fully utilized. Recent work [45], [46] was reported to provide a significant computational saving for an arbitrary order PTFT. A radix-2 decimation-in-frequency (DIF) fast algorithm for any order PTFTs was reported in [45] by using the symmetric properties of the PTFT. The first step of decomposition is to divide the entire computational task into many smaller ones that have equal dimensional sizes, and the second step uses the radix-2 DIF decomposition techniques

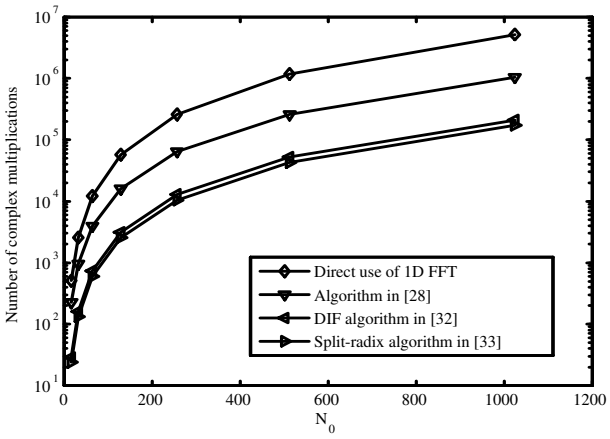

Fig. 1. Multiplicative complexity for 2nd-order PTFT.

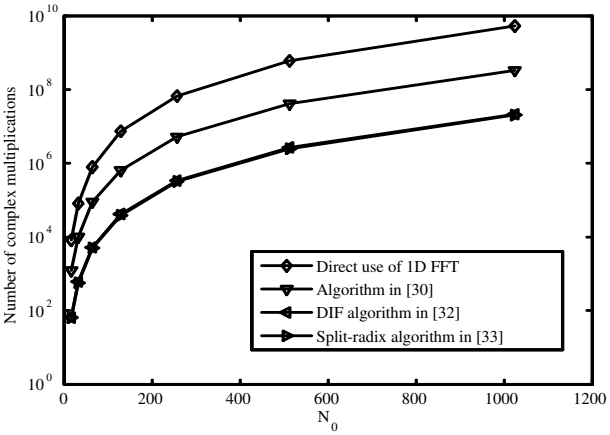

Fig. 2. Multiplicative complexity for 3rd-order PTFT.

to further decompose these smaller PTFTs. This algorithm is simple in concept and easy to implement with significant savings on computational complexity. A general fast algorithm for arbitrary order PTFTs is derived based on the split-radix concept [46]. The algorithm significantly reduces the computational complexity with a simple and regular computational structure which leads to an easy implementation.

To compare the above fast algorithms, for the 2nd-order PTFT, Fig. 1 is given to show the numbers of complex multiplications required by the one directly using 1D FFTs, the fast algorithm in [40], the radix-2 DIF fast algorithm in [45] and the split-radix fast algorithm in [46]. For the 3rd-order PTFT, Fig. 2 shows the numbers of complex multiplications required by the one directly using 1D FFTs, the fast algorithm in [42], the radix-2 DIF fast algorithm in [45] and the split-radix fast algorithm in [46]. The comparisons show that the fast algorithms in [45], [46], which have further explored the properties of the PTFT, can significantly reduce the required number of complex multiplications compared with other reported algorithms.

It should be noted that these reported fast algorithms for PTFT [40], [42], [44]-[46] only support sequence length being a power of two.

When the sequence length is not supported by the available fast algorithms, however, zero padding techniques have to be employed to augment the input sequence to the next available size supported by these fast algorithms. This mismatch surely wastes the computational resources and increases the computational complexity. Therefore fast algorithms based on various radix numbers for other sequence lengths are also highly desired. Based on radix-3 decomposition techniques, fast algorithms for the PTFT of any order is presented in [47]. By combining other factors in the sequence lengths, it can be used to efficiently support many different sequence lengths. The fast algorithms are further generalized for computing the PTFT of length $a^p b$, where a, b and p are positive integers [48]. The symmetric properties of the PTFT are effectively used to minimize the computational complexity. By assigning values of a, b, and p, various algorithms, for example, radix-a and split-radix-2/$(2a)$ are presented to provide the flexibility supporting PTFTs of various sequence lengths. Similarly, fast algorithms for computing the PTFT that deals with a real-valued sequence of length $a^p b$ are investigated in [43]. Since the PTFT has a Hermitian property for real-valued input sequence, the corresponding fast algorithms can effectively reduce the computational complexity compared to the fast algorithms for complex-valued sequences. For example, when $a = 3, 4$ and 8, the computational complexities required by the fast algorithms for real-valued sequences are less than 60% of those needed by the fast algorithms for complex-valued sequences.

V. SNR analysis of the LPFT

In addition to the study of a time-varying frequency content, another important role of the TFRs is that they usually increase the SNR in the time-frequency domain [4]. While random noise tends to spread evenly into the entire time-frequency domain, the signal energy is usually concentrated in a relatively small region. Consequently, the regional SNR could be substantially improved in the time-frequency domain. This feature makes the TFRs to minimize the effect of noises and provide better performance of parameter estimation [4].

Quantitatively analyzing the SNR increase for TFRs is an important issue in practical applications. Generally the SNR is defined as the ratio of the mean power of the signal over the mean power of the noise, where the mean is taken over the whole time domain. Suppose $y(\Omega)$ is a distorted signal

$$y(\Omega) \quad = \quad s(\Omega) + \eta(\Omega), \tag{29}$$

where the variable Ω is in a domain, such as the time domain, the frequency domain or the time-frequency domain, $s(\Omega)$ is the desired signal and $\eta(\Omega)$ is the AWGN with a mean of zero and a variance of σ^2. The SNR is expressed as

$$\mathrm{SNR} = \frac{\int_0^N s^2(\Omega)}{N\sigma^2}, \tag{30}$$

where N is the length of the signal $s(\Omega)$.

According to this SNR definition, an orthogonal transform such as the Fourier transform does not change the SNR [49]. This is because of the energy preservation property of orthogonal transforms. However, this SNR definition in (30) is not suitable to judge the possibility of detecting the narrowband signals in the frequency domain. It is also shown in [49] that this definition is not proper for time-varying signals in the time-frequency domain. For the time-varying signals, we are not interested in the average signal power but in the peak power of the signal.

Another definition of SNR, introduced in [49], is more suitable for signals in the time-frequency domain as well as in the time and frequency domains. Compared with the general SNR definition, this definition is transform-domain dependent and directly relates to the bandwidth of the signal [49].

Following the terminology in [49], the 3dB SNR is defined as the ratio of the 3dB mean power of the signal over the mean power of the noise,

$$\mathrm{SNR}^{3dB} \quad = \quad \frac{\int_ß |s(\Omega)|^2 d\Omega}{|ß|\sigma^2}. \tag{31}$$

Here $|ß|$ is the cardinality of the set ß, with

$$ß = \{t : |s(\Omega)|^2 > 0.5\max|s(\Omega)|^2)\}, \tag{32}$$

where the number 0.5 is from the 3dB bandwidth definition.

The definition of 3dB SNR is the same as the definition in communications, where only the signal in the 3dB bandwidth ß is considered. The superscript $3dB$ is used to represent the SNRs defined in (31) in the rest of the section. Following this transform-domain dependent SNR definition in (31), quantitative analysis on the SNRs achieved by the STFT [49] and the pseudo-WVD [50] has been reported in the literature. Because the TFRs concentrate the time-varying signals better than the FT, the SNR increase in the time-frequency domain is higher than the one in the frequency domain due to the increase of the mean signal power. This property quantitatively explains the advantage of the TFRs over the FT for the ISAR imaging [6], [51].

Compared with the STFT, the local LPFT can further enhance the concentration the LFM signals while spreading the noise. In many different applications [15], [22]-[27], compared with the FT and the STFT, the LPFT has shown its capability for improving the SNR. For example, in radar imaging, the LPFT can achieve more focused and clearer image than that using the STFT in cases of fast maneuvering targets [24], [25]. For nonstationary interference suppression in noise radar systems, the LPFT is able to achieve performance improvement in comparison with that obtained from the systems based on the STFT [71]. Because the SNR analysis of the LPFT will help us to quantitatively evaluate the SNR improvement of the LPFT, here we will give the main results [32].

A. Review on 3dB SNR analysis of the FT and STFT

The 3dB SNR analysis of the FT and STFT has been presented in [49], [51] and will be briefly reviewed in this section. The analysis is based on the LFM signal. As an example, an LFM signal model with monocomponent is considered as:

$$y(t) = s(t) + \eta(t) = Ae^{\left(j(a_1 t + \frac{b_1}{2}t^2)\right)} + \eta(t) \quad (33)$$

where a_1 is the initial frequency, b_1 is the chirp rate of the signal, A is the signal amplitude, and $\eta(t)$ is the additive white Gaussian noise with the correlation function defined as

$$R_\eta(t,\tau) = E[\eta(t)\eta^*(\tau)] = \sigma^2\delta(t-\tau). \quad (34)$$

A.1 3dB SNR analysis of the FT

Suppose $S(f)$ is the Fourier transform of the signal $s(t)$, and B is the bandwidth as $B = \Delta f = |b_1|T$ where T is the time interval. The 3dB mean power of $S(f)$ is less than or equal to [49]

$$\frac{\text{Energy of } S(t)}{B}. \quad (35)$$

Since the Fourier transform is an orthogonal transform which preserves the signal energy, the 3dB SNR in the Fourier transform is

$$\text{SNR}_{FT} \leq \frac{TA^2}{B\sigma^2}. \quad (36)$$

Thus the SNR in the frequency domain for the LFM signal $s(t)$ is

$$\text{SNR}_{FT} \leq \frac{1}{|b_1|} SNR_t, \quad (37)$$

where $\text{SNR}_t = A^2/\sigma^2$ is the SNR of the signal defined in (33).

A.2 3dB SNR analysis of the STFT

Consider the STFT with a Gaussian window function

$$h(t) = (\frac{\alpha}{\pi})^{1/4} e^{(-\frac{\alpha}{2}t^2)}, \qquad \alpha > 0 \quad (38)$$

where α is a parameter controlling the width of the window.

For the LFM signal defined in (33), the STFT can be achieved as [49], [51]

$$|\text{STFT}(s;t,\omega)| =$$

$$= \frac{2A^2\sqrt{\pi}}{\sqrt{\alpha + \frac{1}{\alpha}b_1^2}} e^{\left(\frac{-(\omega - b_1 t - a_1)^2}{\alpha + \frac{1}{\alpha}b_1^2}\right)}. \quad (39)$$

Therefore the 3dB SNR in the STFT domain is [51]

$$\text{SNR}_{STFT}^{3dB} = \frac{1.6\sqrt{\pi}}{\sqrt{\alpha + \frac{1}{\alpha}b_1^2}} \text{SNR}_t. \quad (40)$$

The maximum of the SNR_{STFT}^{3dB}, in terms of the parameter α in (38), is achieved when

$$\alpha = |b_1|, \tag{41}$$

and the maximum is

$$\max_{\alpha}(\text{SNR}_{STFT}^{3dB}) = \frac{0.8\sqrt{2\pi}}{\sqrt{|b_1|}}\text{SNR}_t. \tag{42}$$

Thus,

$$\max_{\alpha}(\text{SNR}_{STFT}^{3dB}) > \text{SNR}_t \quad \text{when} \quad |b_1| < 1.28\pi, \tag{43}$$

which shows the condition that the 3dB SNR in the STFT domain is improved compared with the SNR_t. When the absolute value of the coefficient b_1 is not too large, the SNR in the STFT domain is greater than that in the time domain.

Because the STFT is linear, the above conclusions can be generalized for the signal model containing multiple chirp components with the same mean power defined as

$$\begin{aligned}\tilde{y}(t) &= \sum_{i=1}^{K} s_i(t) + \eta(t) \\ &= \sum_{i=1}^{K} Ae^{(j(a_i t + \frac{b_i}{2}t^2))} + \eta(t),\end{aligned} \tag{44}$$

where $K > 1$, $s_i(t)$ is the ith chirp component, a_i is the initial frequency, b_i is the chirp rate of different signal components and A is the signal amplitude.

The maximum of the SNR_{STFT}^{3dB} is bounded as [51]

$$\frac{0.8\sqrt{2\pi}\text{SNR}_t}{\sqrt{\max_{1\le i\le K}|b_i|}} \le \max_{\alpha}(\text{SNR}_{STFT}^{3dB}) \le \frac{0.8\sqrt{2\pi}\text{SNR}_t}{\sqrt{\min_{1\le i\le K}|b_i|}}, \tag{45}$$

i.e., it is between the maximum and minimum of the components in (42).

The SNR analysis for the STFT using rectangular or Gaussian window function for discrete time signals was obtained in [49] in terms of the sampling rate. For a multicomponent signal with K monocomponents, the SNR in the discrete STFT domain is

$$\text{SNR}_{tf}^{discrete} \approx D\frac{T_0}{K}\frac{N}{T_0}\text{SNR}_t = D\frac{N}{K}\text{SNR}_t, \tag{46}$$

where D is a constant, T_0 is the window length, and N/T_0 is the sampling rate. It can be observed that the SNR improvement in the STFT domain over the SNR in the time domain is in the order of N/K, and the sampling rate plays an important role in the SNR analysis.

B. Quantitative 3dB SNR Analysis of the PWVD

For the WVD defined in (3) the lag variable τ may practically need to be truncated by a short window. Therefore the windowed version of the WVD, which is called the pseudo WVD (PWVD), defined as

$$\text{PWVD}(s;t,\omega) = \int h(\tau)s(t+\tau/2)s^*(t-\tau/2)e^{-j\omega\tau}d\tau, \tag{47}$$

is often employed.

The SNR analysis of the PWVD is presented as follows.Based on the definition of the PWVD in (47), we have

$$\begin{aligned}&\text{PWVD}(y;t,\omega) \\ &= \int h(\tau)s(t+\tau/2)s^*(t-\tau/2)e^{-j\omega\tau}d\tau \\ &\quad + \int h(\tau)N(t;\tau)e^{-j\omega\tau}d\tau.\end{aligned} \tag{48}$$

where

$$\begin{aligned}N(t;\tau) &= \eta(t+\frac{\tau}{2})\eta^*(t-\frac{\tau}{2}) \\ &\quad + s(t+\frac{\tau}{2})\eta^*(t-\frac{\tau}{2}) + \eta(t+\frac{\tau}{2})s^*(t-\frac{\tau}{2}).\end{aligned}$$

On the right-hand side of (48), the first term is the PWVD of the signal and the second term is the PWVD of the noise and cross terms.

Using the Gaussian window function defined in (38), the PWVD of $s(t) = A\exp\left[j(a_1 t + \frac{b_1}{2}t^2)\right]$ is

$$\text{PWVD}(s;t,\omega) =$$

$$= A^2(\frac{\alpha}{\pi})^{1/4}\sqrt{\frac{2\pi}{\alpha}}e^{-\frac{(\omega-a_1-b_1 t)^2}{2\alpha}}. \quad (49)$$

The maximum of the $\text{PWVD}(s;t,\omega)$, achieved with $\omega = a_1 + b_1 t$, is

$$\max_{(t,\omega)}\text{PWVD}(s;t,\omega) = A^2(\frac{\alpha}{\pi})^{1/4}\sqrt{\frac{2\pi}{\alpha}}. \quad (50)$$

Thus the 3dB mean of the PWVD becomes

$$\text{mean}_{(t,\omega)\in ß}\text{PWVD}(s;t,\omega) =$$

$$= 0.8\sqrt{2}A^2(\frac{\pi}{\alpha})^{1/4}. \quad (51)$$

Since the noise $\eta(t)$ is stationary and independent of $s(t)$, the mean power of the noise terms in the PWVD domain is

$$E\left[\int h(\tau)N(t;\tau)e^{-j\omega\tau}d\tau\right] =$$

$$= E[\text{PWVD}(\eta;t,\omega)] = \sigma^2. \quad (52)$$

Thus from (51) and (52) we have

$$\text{SNR}_{PWVD}^{3dB} = 0.8\sqrt{2}(\frac{\pi}{\alpha})^{1/4}\text{SNR}_t,$$

which means that the SNR of the PWVD is controlled by the window parameter α. When $\alpha < 1.6384\pi$, the SNR in the PWVD domain is greater than that in the time domain.

The 3dB SNR analysis for the PWVD has been presented in [50] in discrete-time form, which is expressed by

$$\text{SNR}_{tf}^{discrete} \approx D\frac{N}{K^2}\text{SNR}_t. \quad (53)$$

By comparing (53) with (46), we can observe that the SNR increase for the PWVD is in the order of N/K^2 while that for the STFT is in the order of N/K. This is because the PWVD is a bilinear transform, whereas the STFT is a linear one. K^2 in (53) is due to the cross terms for multicomponents in the PWVD [50].

C. Quantitative 3dB SNR Analysis of the LPFT

Since the LPFT is a linear transformation, the LPFTs of the signal $s(t)$ and the noise $\eta(t)$ can be considered separately.

Using (10), the LPP of the signal is

$$|\text{LPFT}(s;t,\omega)|^2 =$$

$$= \frac{2A^2\sqrt{\pi}}{\sqrt{\alpha+\frac{1}{\alpha}(\omega_1-b_1)^2}}e^{\frac{-(\omega-b_1 t-a_1)^2}{\alpha+\frac{1}{\alpha}(\omega_1-b_1)^2}}. \quad (54)$$

The maximum of $|\text{LPFT}(s;t,\omega,\omega_1)|^2$, achieved at $\omega = b_1 t + a_1$, is

$$\max_{(t,\omega)}|\text{LPFT}(s;t,\omega)|^2 = \frac{2A^2\sqrt{\pi}}{\sqrt{\alpha+\frac{1}{\alpha}(\omega_1-b_1)^2}}. \quad (55)$$

Then,

$$\text{mean}_{(t,\omega)\in S}|\text{LPFT}(s;t,\omega)|^2 =$$

$$= \frac{1.6A^2\sqrt{\pi}}{\sqrt{(\alpha+\frac{1}{\alpha}(\omega_1-b_1)^2)}} \quad (56)$$

Since the noise $\eta(t)$ is stationary, its mean energy can be found in the sample space.

$$E|\text{LPFT}(\eta;t,\omega)|^2 =$$

$$= E|\int \eta(t+s)h(s)e^{-j\omega s}e^{-j\frac{\omega_1}{2}s^2}ds|^2 = \sigma^2.$$

Therefore the 3dB SNR in the LPFT domain is

$$\text{SNR}_{LPFT}^{3dB} = \frac{1.6\sqrt{\pi}}{\sqrt{\alpha+\frac{1}{\alpha}(\omega_1-b_1)^2}}SNR_t \quad (57)$$

where $\text{SNR}_t = A^2/\sigma^2$ is the SNR of the signal defined in (33). The maximum of the SNR_{LPFT}^{3dB}, in terms of the parameter α in (38), is achieved when

$$\alpha = |\omega_1 - b_1| \quad (58)$$

and the maximum is

$$\max_{\alpha}(\text{SNR}_{LPFT}^{3dB}) = \frac{0.8\sqrt{2\pi}}{\sqrt{|\omega_1-b_1|}}\text{SNR}_t. \quad (59)$$

Thus,

$$\max_{\alpha}(\mathrm{SNR}_{LPFT}^{3dB}) > \mathrm{SNR}_t \quad \text{when} \quad \frac{0.8\sqrt{2\pi}}{\sqrt{|\omega_1 - b_1|}} > 1, \tag{60}$$

which shows the condition that the 3dB SNR in the LPFT domain is improved compared with the SNR_t.

The above analysis is for analog LFM signals, but in practical computations, the analog signals need to be sampled. Thus the sampling rate plays an important role in achieving the sufficient resolution. Since the LPFT is a generalized form of the STFT, the LPFT can be obtained by using an STFT procedure, i.e., by sliding the window $h(t)$ over the modulated signal $s(t+\tau)\exp(-j\omega_1\tau^2/2)$, and then implementing the FFT. Therefore, the SNR of the discrete LPFT domain can be expressed as [49],

$$\mathrm{SNR}_{tf}^{discrete} \approx D\frac{T_0}{K}\frac{N}{T_0}\mathrm{SNR}_t = D\frac{N}{K}\mathrm{SNR}_t \tag{61}$$

where D is a constant, K is the number of monocomponents in the signal, T_0 is the window length, and N/T_0 is the sampling rate. Let us discuss the relationship among the SNR, the coefficient $|\omega_{1,i} - b_i|$, the sampling rate, and the window length.

For simplicity, let us consider the following sampled signal

$$s_T(\frac{k}{N}) = e^{(j|\omega_1 - b_1|(T_0 k/N)^2)}, \tag{62}$$

where $k = 0, 1, ..., N-1$. In (62), it is equivalent that the coefficient $|\omega_1 - b_1|$ tends to be zero when the sampling rate N/T_0 tends to be infinity.

For the discrete LPFT of discrete-time signals in (61), the SNR in the LPFT domain tends to be infinity when the sampling rate approaches to infinity. For analog signals, in (59), the SNR in the LPFT domain becomes infinite when the coefficient $|\omega_1 - b_1|$ approaches to zero. As seen from the consideration on the sampled signal, these two results are equivalent, i.e., (61) is equivalent to (59) from the point view of SNR improvement.

Because the LPFT is linear, the above conclusions can be generalized for the signal model containing multiple chirp components with the same mean power defined in (44). The maximum of the $\mathrm{SNR}_{LPFT}^{3dB}$ is bounded as

$$\frac{0.8\sqrt{2\pi}\mathrm{SNR}_t}{\sqrt{\max_{1\le i\le K}|\omega_{1,i} - b_i|}} \le \max_{\alpha}(\mathrm{SNR}_{LPFT}^{3dB}) \le \frac{0.8\sqrt{2\pi}\mathrm{SNR}_t}{\sqrt{\min_{1\le i\le K}|\omega_{1,i} - b_i|}}, \tag{63}$$

where $\omega_{1,i}$ denotes the chirp rate of LPFT of the ith component.

It is worth nothing that when ω_1 is set to zero, the LPFT becomes the STFT, and the quantitative analisys for the LPFT becomes that for the STFT as given in [51].

D. Comparisons

In this section, the LPFT is compared with the FT, the STFT and the WVD in SNR analysis to show that the LPFT can achieve better SNR performance than the FT, the STFT and the WVD.

The maximum of the $\mathrm{SNR}_{LPFT}^{3dB}$, achieved with $\alpha = |\omega_1 - b_1|$, is

$$\max_{\alpha}(\mathrm{SNR}_{LPFT}^{3dB}) = \frac{0.8\sqrt{2\pi}}{\sqrt{|\omega_1 - b_1|}}\mathrm{SNR}_t. \tag{64}$$

Because the 3dB SNR in the frequency domain is $\mathrm{SNR}_{FT}^{3dB} \le \frac{1}{|b_1|}\mathrm{SNR}_t$ [51], we have

$$\max_{\alpha}(\mathrm{SNR}_{LPFT}^{3dB}) > \mathrm{SNR}_{FT}^{3dB} \quad \text{when} \quad \frac{0.8\sqrt{2\pi}|b_1|}{\sqrt{|\omega_1 - b_1|}} > 1, \tag{65}$$

which shows the condition that the 3dB SNR in the LPFT domain is improved compared with the SNR in the Fourier transform domain.

The maximum 3dB SNR in the STFT domain was [51]

$$\max_{\alpha'}(\mathrm{SNR}_{STFT}^{3dB}) = 0.8\frac{\sqrt{2\pi}}{\sqrt{b_1}}\mathrm{SNR}_t, \tag{66}$$

where $\alpha' = |b_1|$, which is optimal to achieve the maximum of $\mathrm{SNR}^{3dB}_{STFT}$. From (64) and (66), we have

$$\frac{\max_\alpha(\mathrm{SNR}^{3dB}_{LPFT})}{\max_{\alpha'}(\mathrm{SNR}^{3dB}_{STFT})} = |\frac{b_1}{\omega_1 - b_1}| \tag{67}$$

which indicates that as long as $|\frac{b_1}{\omega_1 - b_1}| > 1$, the maximum of $\mathrm{SNR}^{3dB}_{LPFT}$ is larger than $\mathrm{SNR}^{3dB}_{STFT}$. When $\omega_1 = b_1$, the ratio in (67) becomes infinity, which means that the method based on the LPFT can achieve a significantly higher SNR than that based on the STFT.

The 3dB SNR achieved by the PWVD has been presented as

$$\mathrm{SNR}^{3dB}_{PWVD} = 0.8\sqrt{2}(\frac{\pi}{\alpha})^{1/4}\mathrm{SNR}_t,$$

Thus, we have

$$\frac{\max_\alpha(\mathrm{SNR}^{3dB}_{LPFT})}{\mathrm{SNR}^{3dB}_{PWVD}} = \left(\frac{\pi}{|\omega_1 - b_1|}\right)^{1/4} \tag{68}$$

which means that as long as $|\omega_1 - b_1| \leq \pi$, or $b_1 - \pi \leq \omega_1 \leq b_1 + \pi$, a higher $\mathrm{SNR}^{3dB}_{LPFT}$ than $\mathrm{SNR}^{3dB}_{PWVD}$ is obtained. Furthermore, when ω_1 is estimated correctly, the parameter $\alpha = |\omega_1 - b_1|$ approaches to zero. Under this condition, the maximum $\mathrm{SNR}^{3dB}_{LPFT}$ approaches to infinity.

For the signal model containing multiple chirp components with the same mean power which is defined in (44), the maximum of the $\mathrm{SNR}^{3dB}_{LPFT}$ is bounded as

$$\frac{0.8\sqrt{2\pi}\mathrm{SNR}_t}{\sqrt{\max_{1\leq i\leq K}|\omega_{1,i} - b_i|}} \leq \max_\alpha(\mathrm{SNR}^{3dB}_{LPFT})$$

$$\leq \frac{0.8\sqrt{2\pi}\mathrm{SNR}_t}{\sqrt{\min_{1\leq i\leq K}|\omega_{1,i} - b_i|}}, \tag{69}$$

clearly we have

$$\max_\alpha(\mathrm{SNR}^{3dB}_{LPFT}) > \mathrm{SNR}_t$$

when

$$\max_{1\leq i\leq K}|\omega_{1,i} - b_i| < 1.28\pi. \tag{70}$$

As shown in [51] that 3dB SNR in the frequency domain is $\mathrm{SNR}^{3dB}_{FT} \leq \frac{1}{|b_i|}\mathrm{SNR}_t$, we have

$$\max_\alpha(\mathrm{SNR}^{3dB}_{LPFT}) > \mathrm{SNR}^{3dB}_{FT}$$

when

$$\frac{0.8\sqrt{2\pi}|b_i|}{\sqrt{|\omega_{1,i} - b_i|}} > 1. \tag{71}$$

It is shown that for the multiple chirp signal model, $\mathrm{SNR}^{3dB}_{STFT}$ is [51]

$$\max_{\alpha'_i}(\mathrm{SNR}^{3dB}_{STFT}) = 0.8\frac{\sqrt{2\pi}}{\sqrt{b_i}}\mathrm{SNR}_t.$$

where $\alpha'_i = |b_i|$.

Thus for multiple chirp signals the condition for

$$\max_{\alpha_i}(\mathrm{SNR}^{3dB}_{LPFT}) > \max_{\alpha'_i}(\mathrm{SNR}^{3dB}_{STFT})$$

is

$$\frac{|b_i|}{\max_{1\leq i\leq K}|\omega_{1,i} - b_i|} > 1.$$

It can be concluded that as long as ω_1 is estimated correctly, the use of LPFT indeed achieves a significant performance improvement compared to those achieved by using the FT and the STFT.

For signals having multiple components, the WVD generally has cross terms that often lead to incorrect interpretation of signal content. The LPFT, as a linear transform, is free from the cross terms. Therefore, the LPFT of signals having multiple components can still achieve higher 3dB SNR than the WVD.

E. Simulations

In this section, simulation results are presented to verify the theoretical analysis presented in the above sections. The simulation uses the signal $y(t) = \exp[j(2t + 8t^2)] + \eta(t)$ with a sampling rate 333 Hz and $\mathrm{SNR}_t = -3$dB. Fig. 3 shows that the maximum 3dB SNR is obtained when $\omega_1 = 16$, which indicates that the 3dB SNR in the time-frequency domain reaches the maximum value when the

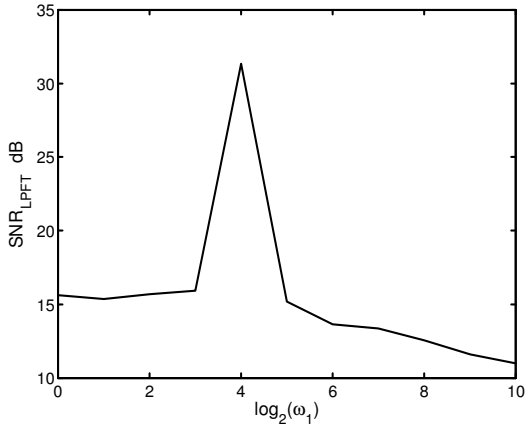

Fig. 3. The $\mathrm{SNR}_{LPFT}^{3dB}$ versus ω_1.

chirp rate of LPFT ω_1 matches the signal chirp rate b_1.

Fig. 4 presents the ratio between $\mathrm{SNR}_{LPFT}^{3dB}$ and SNR_{FT}^{3dB}, the ratio between $\mathrm{SNR}_{LPFT}^{3dB}$ and $\mathrm{SNR}_{STFT}^{3dB}$, and the ratio between $\mathrm{SNR}_{LPFT}^{3dB}$ and $\mathrm{SNR}_{PWVD}^{3dB}$, respectively. In the figure, the simulation results (solid curves) closely match the theoretical results (dashed curves). More importantly, the figure illustrates that the maximum gain in SNR is achieved when the chirp rate ω_1 used by the LPFT matches the signal chirp rate b_1, compared with those achieved by using the FT, the STFT and the PWVD.

It should be noted that the SNR analysis for the LPFT is based on the LFM signals. As stated in Section III, for other kind of time-varying signals such as sinusoidal frequarncy modulated (FM) signals or parabolic FM signals, we can use the window function to segment the signals so that each segment within the window can be assumed to be the LFM signal. In this way, the LPFT can be used to process the higher-order time-varying signals and achieve high SNR improvement. Consider a parabolic FM signal $s(t) = \exp[j2\pi(0.4t - 0.00135t^2 + 0.0000173t^3)]$ with $\mathrm{SNR}_t = -3$dB. Fig. 5 presents the parabolic FM signal in different domains. It can be seen that the LPFT can provide improved SNR performance than the methods in other domains such as time domain, frequency domain, STFT domain and WVD domain. As shown in Fig. 6, for the signals with multiple chirp components which is defined as $s(t) = \exp[j2\pi(0.000481t^2)] + \exp[j2\pi(0.5t - 0.000481t^2)]$, the LPFT can also give improved SNR performance than the methods in other domains.

It should be noted that this section focuses on the 3dB SNR analysis of the LPFT compared with that of the FT, STFT and PWVD, using the 3dB SNR definition in [49]-[51]. The influence of the noise in the time-frequency domain for the STFT and bilinear distributions from the Cohen's class can also be presented in terms of the output SNR, as shown in [52], [53]. Furthermore, expressions of the bias and variance for the STFT and bilinear distributions as IF estimators are discussed in [54], [55]. These results have been generalized to the LPFT in [22], [23] and [27], respectively.

VI. The reassigned local polynomial periodogram

The reassignment method is an effective operation to improve signal concentration in the time-frequency domain. It has been generalized to deal with the bilinear time-frequency and time-scale distributions [56], the affine class [57] and S-method [58]. More detailed information on the reassignment method can be found in [56], [59], [60].

The LPFT has been combined with the reassignment method to improve the resolution in the time-frequency domain [61], and its definition and properties have also been discussed. In this section, we will give a review on the reassigned LPP, and then the reassignment method is extended to the robust spectrogram and LPP to improve the concentration for signals corrupted by impulsive noises. Furthermore, performance using various LPP-related methods are compared for signals in different noise environments.

A. Review on the reassignment method

As introduced in [3], the spectrogram (SP), WVD, smoothed pseudo-WVD (SPWVD) and many other bilinear counterparts can be written in a general form, known as the Cohen's

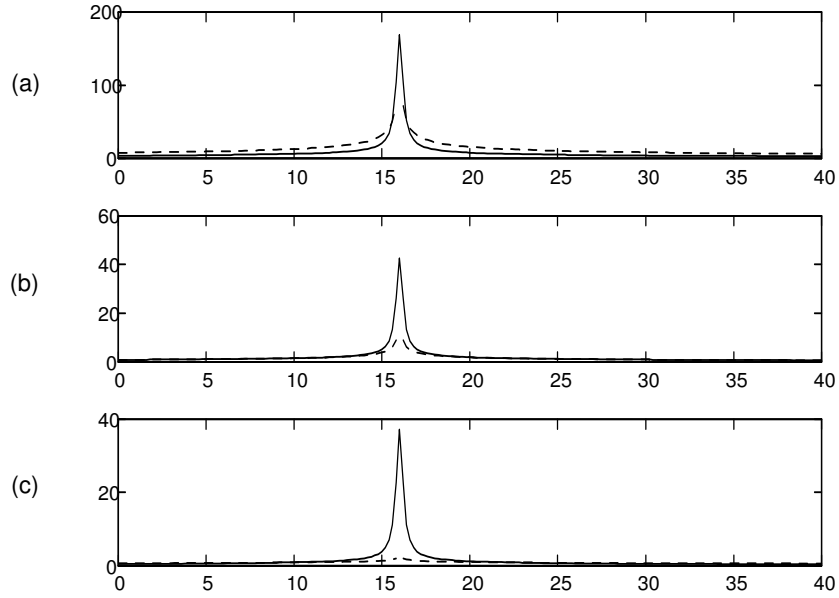

Fig. 4. (a) is the ratio between $\mathrm{SNR}_{LPFT}^{3dB}$ and SNR_{FT}^{3dB}, (b) is the ratio between $\mathrm{SNR}_{LPFT}^{3dB}$ and $\mathrm{SNR}_{STFT}^{3dB}$, and (c) is the ratio between $\mathrm{SNR}_{LPFT}^{3dB}$ and $\mathrm{SNR}_{PWVD}^{3dB}$.

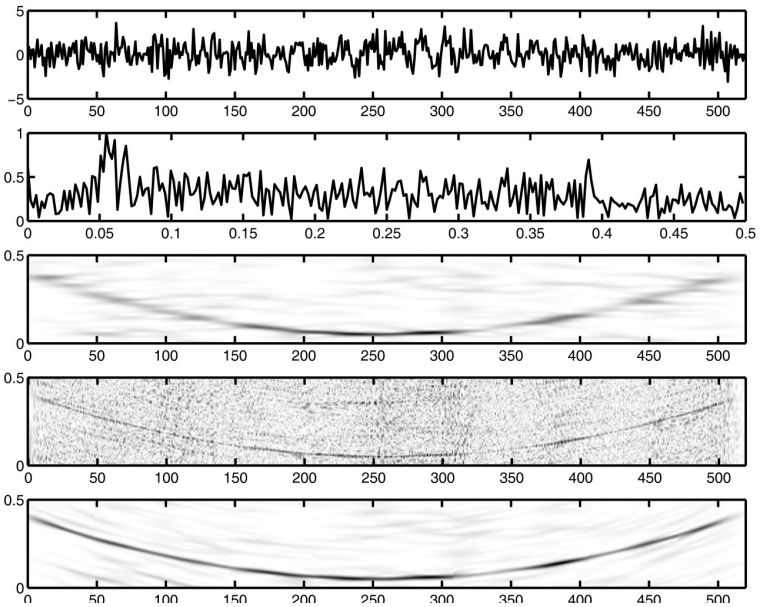

Fig. 5. The representations of the parabolic FM signal in different domains. From top to bottom: time domain, frequency domain, STFT domain, WVD domain, and LPFT domain. SNR = −3dB.

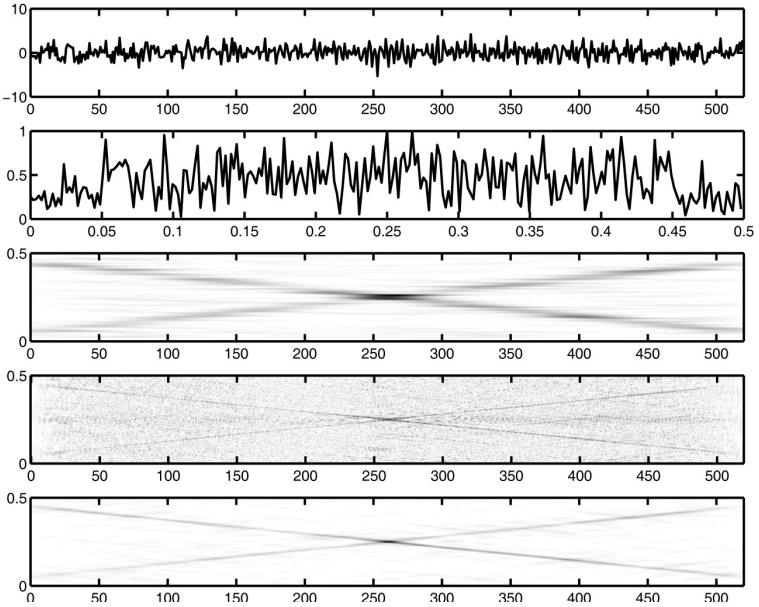

Fig. 6. The representations of a signal with multiple components in different domains. From top to bottom: time domain, frequency domain, STFT domain, WVD domain, and LPFT domain. SNR = 0dB.

class, expressed as [4]

$$\mathrm{TFR}(x;t,\omega) = \\ = \frac{1}{4\pi^2}\int\int \phi(u,\Omega)\mathrm{WVD}(x;t-u,\omega-\Omega)dud\Omega, \tag{72}$$

where $\mathrm{WVD}(x;t,\omega)$ is the WVD of a given signal $x(t)$ and $\phi(u,\Omega)$ is the distribution kernel which determines the distribution and its properties. Many members in the Cohen's class are able to suppress the cross terms of the WVD, but with undesirable effects of broadening the signal components in the time-frequency domain. In order to minimize such undesirable effects, a reassigned time-frequency representation (RTFR) is used to improve the concentration of the signal component by reallocating its energy distribution in the time-frequency domain. By moving the attribution point of the average operation to the gravitational center of the energy contribution, the RTFR is defined as

$$\mathrm{RTFR}(x;t',\omega') = \\ = \int\int \mathrm{TFR}(x;t,\omega)\delta(t'-\hat{t}(x;t,\omega)) \\ \times\delta(\omega'-\hat{\omega}(x;t,\omega))dtd\omega, \tag{73}$$

where $\hat{t}(x;t,\omega)$ and $\hat{\omega}(x;t,\omega)$ are the coordinates of the gravitational center, by way of analogy to a mass distribution.

For the well known SP, the reassignment operators of its reassigned form, the RSP, are given by eq. 74 and eq. 75, [59], where Re and Im indicate the real part and imaginary part, respectively, and the subscripts h, Th and Dh indicate that the associated STFTs use the window $h(t)$, the time ramped window $t\cdot h(t)$, and the first derivative of the window $\frac{dh(t)}{dt}$, respectively.

B. The Reassigned LPP

We will consider the definitions of the reassignment methods based on the second-order LPP. Since ω_1 can be estimated from the PTFT, the LPP is a bilinear TFR and the reassignment method can be extended to the LPP to obtain performance improvement [62]. Therefore, the RLPP is defined by eq. 76.

The expressions of the reassignment operators for the RLPP are given in (77) and (78), and its proof can be referred to [61].

$$\begin{aligned}\hat{t}(x;t,\omega) &= t - \frac{\int\int u\,\mathrm{WVD}\,(h;u,\Omega)\,\mathrm{WVD}\,(x;t-u,\omega-\Omega)\,dud\Omega}{\int\int \mathrm{WVD}\,(h;u,\Omega)\,\mathrm{WVD}\,(x;t-u,\omega-\Omega)\,dud\Omega} \\ &= t - \mathrm{Re}\left\{\frac{\mathrm{STFT}_{Th}(x;t,\omega)}{\mathrm{STFT}_h(x;t,\omega)}\right\} \end{aligned} \tag{74}$$

$$\begin{aligned}\hat{\omega}(x;t,\omega) &= \omega - \frac{\int\int \Omega\,\mathrm{WVD}\,(h;u,\Omega)\,\mathrm{WVD}\,(x;t-u,\omega-\Omega)\,dud\Omega}{\int\int \mathrm{WVD}\,(h;u,\Omega)\,\mathrm{WVD}\,(x;t-u,\omega-\Omega)\,dud\Omega} \\ &= \omega + \mathrm{Im}\left\{\frac{\mathrm{STFT}_{Dh}(x;t,\omega)}{\mathrm{STFT}_h(x;t,\omega)}\right\}, \end{aligned} \tag{75}$$

$$\mathrm{RLPP}(x;t',\omega') = \int\int \mathrm{LPP}\,(x;t,\omega)\,\delta\left(t'-\hat{t}(x;t,\omega)\right)\delta\left(\omega'-\hat{\omega}\,(x;t,\omega)\right)dtd\omega. \tag{76}$$

$$\hat{t}(x;t,\omega) = t - \frac{\int\int u\,\mathrm{WVD}\left(h;u,-\frac{\omega_1}{2}u+\Omega\right)\mathrm{WVD}\left(x;t-u,\omega-\frac{\omega_1}{2}u-\Omega\right)dud\Omega}{\int\int \mathrm{WVD}\left(h;u,-\frac{\omega_1}{2}u+\Omega\right)\mathrm{WVD}\left(x;t-u,\omega-\frac{\omega_1}{2}u-\Omega\right)dud\Omega}$$

$$= t - \mathrm{Re}\left\{\frac{\mathrm{LPFT}_{Th}(x;t,\omega)\ \mathrm{LPFT}_h^*(x;t,\omega)}{|\mathrm{LPFT}_h(x;t,\omega)|^2}\right\} = t - \mathrm{Re}\left\{\frac{\mathrm{LPFT}_{Th}(x;t,\omega)}{\mathrm{LPFT}_h(x;t,\omega)}\right\} \tag{77}$$

$$\hat{\omega}(x;t,\omega) = \omega - \frac{\int\int \left\{\begin{array}{l}\left(\Omega-\frac{\omega_1}{2}u\right)\ \mathrm{WVD}\left(h;u,-\frac{\omega_1}{2}u+\Omega\right) \\ \cdot\mathrm{WVD}\left(x;t-u,\omega-\frac{\omega_1}{2}u-\Omega\right)\end{array}\right\}dud\Omega}{\int\int \mathrm{WVD}\left(h;u,-\frac{\omega_1}{2}u+\Omega\right)\mathrm{WVD}\left(x;t-u,\omega-\frac{\omega_1}{2}u-\Omega\right)dud\Omega}$$

$$= \omega + \mathrm{Im}\left\{\frac{\mathrm{LPFT}_{Dh}(x;t,\omega)\ \mathrm{LPFT}_h^*(x;t,\omega)}{|\mathrm{LPFT}_h(x;t,\omega)|^2}\right\} = \omega + \mathrm{Im}\left\{\frac{\mathrm{LPFT}_{Dh}(x;t,\omega)}{\mathrm{LPFT}_h(x;t,\omega)}\right\} \tag{78}$$

Because the WVD is always real-valued, the reassignment operators in (77) and (78) are also real-valued. It is noted that when $\omega_1 = 0$, the LPFT becomes the STFT, and the reassignment operators of the LPP in (77) and (78) become those of the RSP as in (74) and (75).

Since the RLPP has similar reassignment operators as that of the RSP, they share the same properties, such as nonnegativity, nonbilinearity, time and frequency shifts invariance, time-scaling property, symmetry, energy conservation, and perfect localization on chirp and impulse signals. The properties of the RLPP can be derived from (77) and (78). Some of their proofs are presented in [61].

There are two simplified variations of the RLPP. One is the reassigned LPP along the frequency direction (RfLPP), defined as:

$$\mathrm{RfLPP}(x;t,\omega') =$$

$$= \int \mathrm{LPP}(x;t,\omega)\delta[\omega'-\hat{\omega}(x;t,\omega)]d\omega, \tag{79}$$

in which no reassignment is made in the time direction. The other one is the reassigned LPP along the time direction (RtLPP), defined as:

$$\text{RtLPP}(x;t',\omega) =$$

$$= \int \text{LPP}(x;t,\omega)\delta[t' - \hat{t}(x;t,\omega)]dt, \quad (80)$$

in which no reassignment is made in the frequency direction.

The RfLPP and RtLPP share with the RLPP on the properties of nonnegativity, nonbilinearity, time-scaling, energy conservation, time folding and symmetry. Moreover, the RfLPP particularly has the properties of frequency shift invariance and perfectly localizing the chirp components, while the RtLPP has the properties of time shift invariance and perfectly localizing the impulse components. It means that the RfLPP is responsible for perfectly localizing the chirps and the RtLPP is for perfectly localizing the impulse, as shown by the simulations in [61]. Simulations for signals with chirp or/and impulse components, as well as for other higher-order signals with multicomponents, can also be referred to [61].

C. The Reassigned Robust LPP

In practice, the signals under consideration are always embedded in noise. For signals corrupted by AWGN, the required performance can be achieved with the standard methods, such as the STFT and the LPFT [39]. However, in some situations such as in the applications of communications and imaging, signals are corrupted by impulsive noise. In this case, these standard methods have difficulties in obtaining sufficient signal concentration and resolution. To minimize the effects of impulsive noise, Huber proposed the robust estimation methods to obtain the parameters of the corrupted signals [7]. The robust STFT based on median filtering [63] was also introduced recently to achieve significantly better performance in impulsive noise environments. Similarly, the robust LPFT was proposed to produce highly concentrated representations of time-varying signals in impulsive noise [34].

C.1 Review on the Robust Methods

The STFT form of a signal $x(t)$ is defined by the following minimization problem [7]:

$$\text{STFT}(t,\omega) = \arg\min_m J(t,\omega;m), \quad (81)$$

where

$$J(t,\omega,m) = \sum_n h(nT)F[e(t,\omega,n;m)], \quad (82)$$

$h(nT)$ is a real and even window function, $F(e)$ is a loss function and $e(t,\omega,n;m)$ is the error function given by

$$e(t,\omega,n;m) = x(t+nT)e^{-j\omega nT} - m, \quad (83)$$

where T is the sampling period and m is an estimated expectation of the sample average of $x(t+nT)\ e^{-j\omega nT}$.

The standard STFT is a solution to (81) with a loss function $F(e) = |e|^2$. With the loss function $F(e) = |e|$ or $F(e) = |\text{Re}(e)|+|\text{Im}(e)|$, the robust M-STFT [64] or the robust STFT with the median filtering [63] can be obtained. The computation of the robust M-STFT needs the iterative procedures and therefore generally requires a heavy computational load [64]. The robust STFT with the median filtering has a simpler solution because it uses a sorting procedure [63]. Therefore the robust method based on median filtering is employed in this section. The robust STFT is defined as [63]

$$\text{rSTFT}(t,\omega) =$$

$$= \text{median}\{\text{Re}[x(t+nT)h(nT)e^{-j\omega nT}]\}$$

$$+j\text{median}\{\text{Im}[x(t+nT)h(nT)e^{-j\omega nT}]\}. \quad (84)$$

The robust spectrogram is defined as $|\text{rSTFT}|^2$.

The robust LPFT of the input $x(t)$ is defined as [34]:

$$\text{rLPFT}(t,\omega,\omega_1) =$$

$$= \text{median}\{\text{Re}[x(t+nT)h(nT)e^{-j\omega nT-\frac{j\omega_1(nT)^2}{2}}]\}$$

$$+j\text{median}\{\text{Im}[x(t+nT)h(nT)e^{-j\omega nT-\frac{j\omega_1(nT)^2}{2}}]\}. \quad (85)$$

In this case, the robust PTFT is used to estimate ω_1 for signals corrupted by impulsive

noise. The estimation performances achieved by using the PTFT and robust PTFT of the signals in impulsive noise were compared in [39]. It was shown that the peaks from the robust PTFT are more easily identified than from the PTFT. Similarly the robust LPP is defined as $|\text{rLPFT}|^2$.

C.2 Definition of the Reassigned robust SP and LPP

The reassignment method is extended to the robust spectrogram and the robust LPP to obtain a good distribution concentration for signals embedded in impulsive noise. The operators of the reassigned robust spectrogram (RrSP) are defined as:

$$\hat{t}(x;t,\omega) = t - \text{Re}\left\{\frac{\text{rSTFT}_{Th}(x;t,\omega)}{\text{rSTFT}_h(x;t,\omega)}\right\}, \quad (86)$$

$$\hat{\omega}(x;t,\omega) = \omega + \text{Im}\left\{\frac{\text{rSTFT}_{Dh}(x;t,\omega)}{\text{rSTFT}_h(x;t,\omega)}\right\}. \quad (87)$$

The reassignment operators of the reassigned robust LPP (RrLPP) are defined as:

$$\hat{t}(x;t,\omega) = t - \text{Re}\left\{\frac{\text{rLPFT}_{Th}(x;t,\omega)}{\text{rLPFT}_h(x;t,\omega)}\right\}, \quad (88)$$

$$\hat{\omega}(x;t,\omega) = \omega + \text{Im}\left\{\frac{\text{rLPFT}_{Dh}(x;t,\omega)}{\text{rLPFT}_h(x;t,\omega)}\right\}. \quad (89)$$

The reassigned robust LPP along the frequency direction (RfrLPP) is given by:

$$\text{RfrLPP}(x;t,\omega') =$$

$$= \int \text{rLPP}(x;t,\omega)\delta[\omega' - \hat{\omega}(x;t,\omega)]d\omega.$$

In general, the use of the robust LPFT in robust LPP is similar to the use of the robust STFT in the robust spectrogram. One additional requirement for the robust LPFT is that the parameter ω_1 in (85) has to be estimated from the robust PTFT of each signal segment.

D. Performance Comparisons

Let us compare the performances of those LPP-related methods discussed above in terms of the readability of signal components, the required computational complexity, the ratio of distribution concentration, and the mean squared errors (MSEs) of the IF estimation.

The testing signal follows a parabolic FM law,

$$x(t) = e^{j2\pi(0.5t - 0.00173t^2 + 0.0000022t^3)}, \quad (90)$$

which is assumed to be corrupted by impulsive noise, $n(t) = \alpha[w_1^3(t) + jw_2^3(t)]$, where $\alpha = 0.5$, $w_1(t)$ and $w_2(t)$ are independent Gaussian random variables with unit variances. The variance of the impulsive noise is $\sigma_n^2 = 30\alpha^2$ [65], leading to a SNR of -1.85dB when $\alpha = 0.5$. The probability density function of the noise is $g(x) = 1/3\sqrt{2\pi}e^{-|x|^{2/3}/2}|x|^{-2/3}$, which was used to model many real-life engineering problems [34] [63]. A Hamming window of 65 points is used in the simulations. Within the window duration, each signal segment of the signal can be approximately assumed to be a chirp.

D.1 Readability

Fig. 7(a) shows the standard spectrogram of a clean signal $x(t)$ and Fig. 7(b) gives the standard spectrogram of the signal corrupted by impulsive noise. The robust spectrogram of the corrupted signal is given in Figure 7(c) to show the improvement on signal concentration compared with that in Fig. 7(b). Finally, Figure 7(d) gives the reassigned robust spectrogram of the signal in the same noise environment. Although better visual representation on the signal component is achieved by applying the reassignment and robust operations to the spectrogram, further improvements on signal concentration and resolution in the time-frequency domain are still desired for practical applications.

We now consider the LPP-related representations for the same corrupted signal, as shown in Fig. 8. The comparison between Fig. 7(b) and Figure 8(a) shows that the latter achieves an obvious improvement on signal concentration, which is expected because the LPP uses the parameter ω_1 to more accurately describe the change of the signal frequencies. It is also observed that in Fig. 8(b) the robust LPP achieves a substantial improvement on signal representation in the time-frequency domain. Furthermore, Figures 8(c) and (d) show that the reassignment operations on the robust

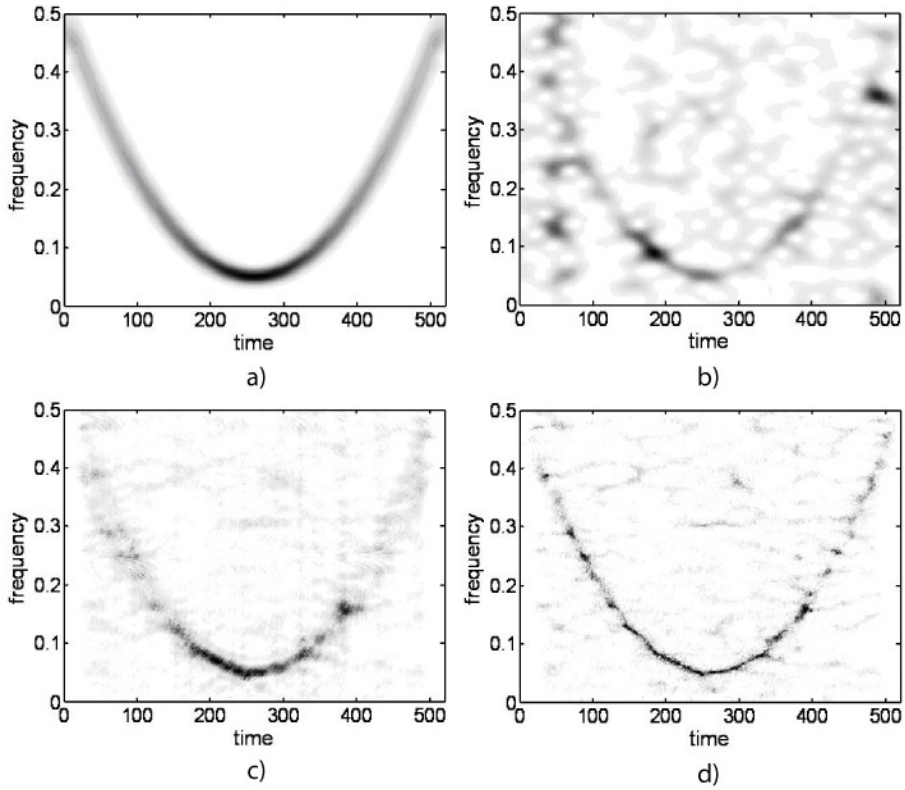

Fig. 7. The spectrogram-related representations of the signal in impulsive noise; (a) spectrogram of a clean signal, (b) spectrogram of a corrupted signal, (c) robust spectrogram of a corrupted signal and (d) reassigned robust spectrogram of a corrupted signal.

LPP are effective to improve the concentration in the time-frequency domain. The RfrLPP in Figure 8(d) appears to be more concentrated than the RrLPP in Fig. 8(c).

Both Fig. 7 and Fig. 8 show that, compared with the standard methods, the robust SP and robust LPP using median filtering are effective to remove the effects of impulsive noise. Then with the reassignment operations, the concentration of the signal component can be further improved.

Fig. 9 and Fig. 10 show the representations based on the SP and LPP, respectively, for signal $x(t)$ embedded in AWGN $n(t) = 0.75[w_1(t) + jw_2(t)]$. Again, it is seen that the LPP-related representations achieve better performances than their spectrogram-related counterparts. It is also observed that the RrLPP in Figure 10(b) achieves slightly degraded representation than the RLPP in Fig. 10(e). It is because it is not useful for minimizing the effects of AWGN although the median filtering used in robust methods is effective to reduce the effects of impulsive noise. This observation is consistent with the conclusion in [34]. Meanwhile, Fig. 9 and Figure 10 show that all the reassigned representations achieve improvement on signal concentration compared with their counterparts without the reassignment. In particular, both the RfrLPP in Fig. 10 (c) and the RfLPP in Figure 10(f) achieve sufficiently concentrated representations.

D.2 Computational complexity

For the spectrogram-related methods that are used for Fig. 7 and Fig. 9, the maximum overlap between adjacent segments is necessary to achieve good signal representations. The maximum overlap is accomplished

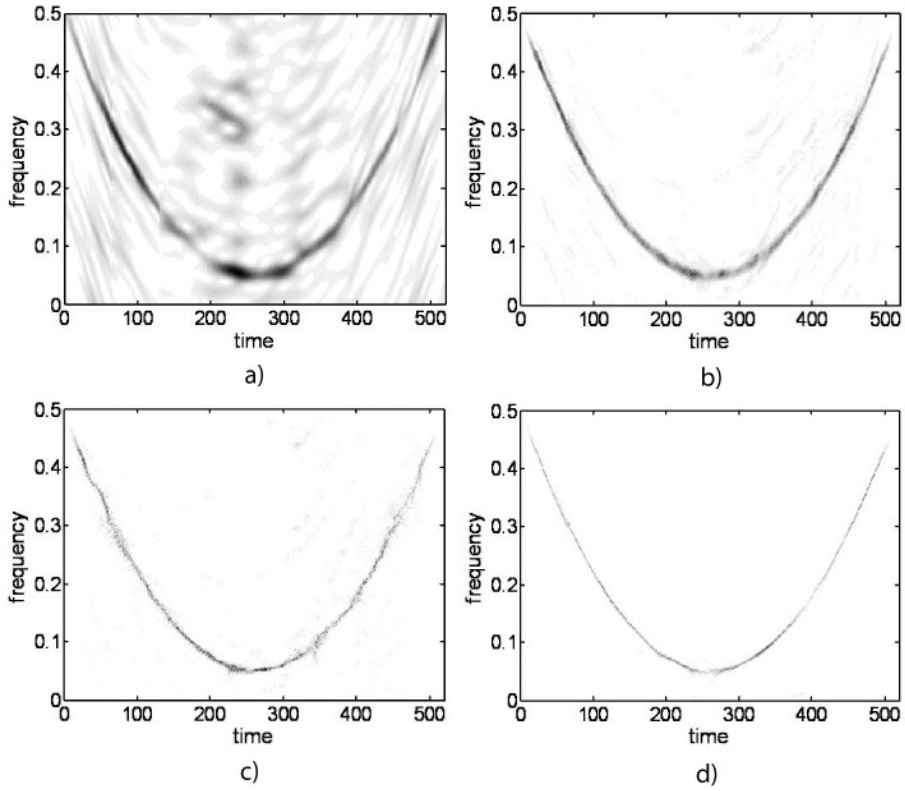

Fig. 8. The LPP-related representations of the signal in impulsive noise; (a) LPP, (b) robust LPP, (c) reassigned robust LPP, and (d) reassigned robust LPP along the frequency direction.

by sliding the window by one data point to obtain each succeeding signal segment. It was reported in [39] that even without any overlap between adjacent segments, a good approximation to the signal components can be achieved by the LPFT as long as the window is short enough, as demonstrated in Figure 8 and Fig. 10. For the sake of comparison, Fig. 11 gives the LPP and RLPP that are computed with the maximum overlap. Visual inspections show that the LPP and RLPP in Figure 11(a) and (b) are not obviously better than those without any overlap in Fig. 10 (d) and (e). However the process without any overlap greatly reduces the computational complexity, which is shown later in Table I. In the LPP without overlap, each segment within the small window is assumed to be a chirp having the same parameter ω_1. When the chirp rates of the consecutive segments are sufficiently different, smearing in the time-frequency domain may occur between the segments.

A window of length L is used to segment the signal, and therefore, each segment needs an L-point Fourier transform whose computational complexity, in terms of the number of complex multiplications, is in the order of $L \log_2 L$. For the spectrogram of an N-point signal sequence, where $N >> L$ and the maximum overlap is used, the computational complexity is in the order of $NL \log_2 L$. The LPP computation for each data segment needs to estimate the parameter ω_1 by using the PTFT, which requires a computational complexity in the order of LL_1 [45], where L and L_1 are the number of points related to ω and ω_1, or the dimensional sizes of the PTFT, respectively. According to the result reported in [40], L_1 should be larger than L to achieve a satisfactory accuracy. Since the LPP, with an esti-

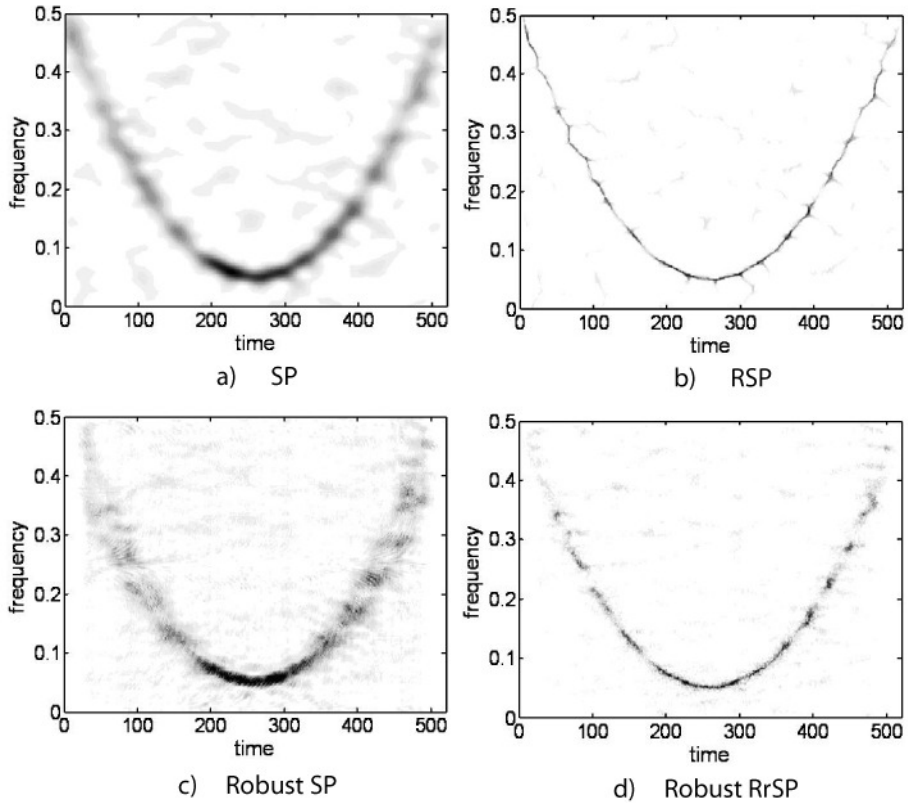

Fig. 9. The spectrogram-related representations of a signal in AWGN.

mated ω_1, is performed in the same way as the spectrogram, the total numbers of complex multiplications for the LPP of an N-point sequence are in the orders of $NL(\log_2 L + L_1)$ for the maximum overlap, and $N(L \log_2 L + L_1)$ for nonoverlap between the segments, respectively.

For the reassigned methods such as the RLPP and RSP, most of the computational complexity is for the reassignment process. Therefore, the RLPP does not need much more computational complexity than the RSP. Since the computational complexity of the sorting procedure, i.e., the quick sorting algorithm [66], for the robust methods is in the order of $L \log_2 L$, the computational complexity of the robust spectrogram is in the order of $N^2 L \log_2 L$. Therefore using the robust PTFT to estimate the parameter ω_1, the computational complexity of the robust LPP without overlap is in the order of $NL(N + L_1) \log_2 L$. The main computational complexity for the RrLPP is for the sorting procedure of the median filtering. The computational complexity of the RrLPP is about three times of that needed by the robust LPP since the reassignment computation needs about three times of that for the sorting procedure compared to the robust LPP.

The computation times required by various methods for the specific signal $x(t)$ are listed in Table I. The signal is corrupted by either AWGN or impulsive noise when the robust operation is applied in the processing methods. The computations are under the programming environment of MATLAB 7.1. The computer is Pentium 4 with a clock rate of 2.66 GHz and a RAM size of 512 MBytes. The numerical values in Table I are the average of 50 measurements of the computation times. The computation times of LPP and RLPP with the maximum overlap are 38.86 and 41.57 seconds,

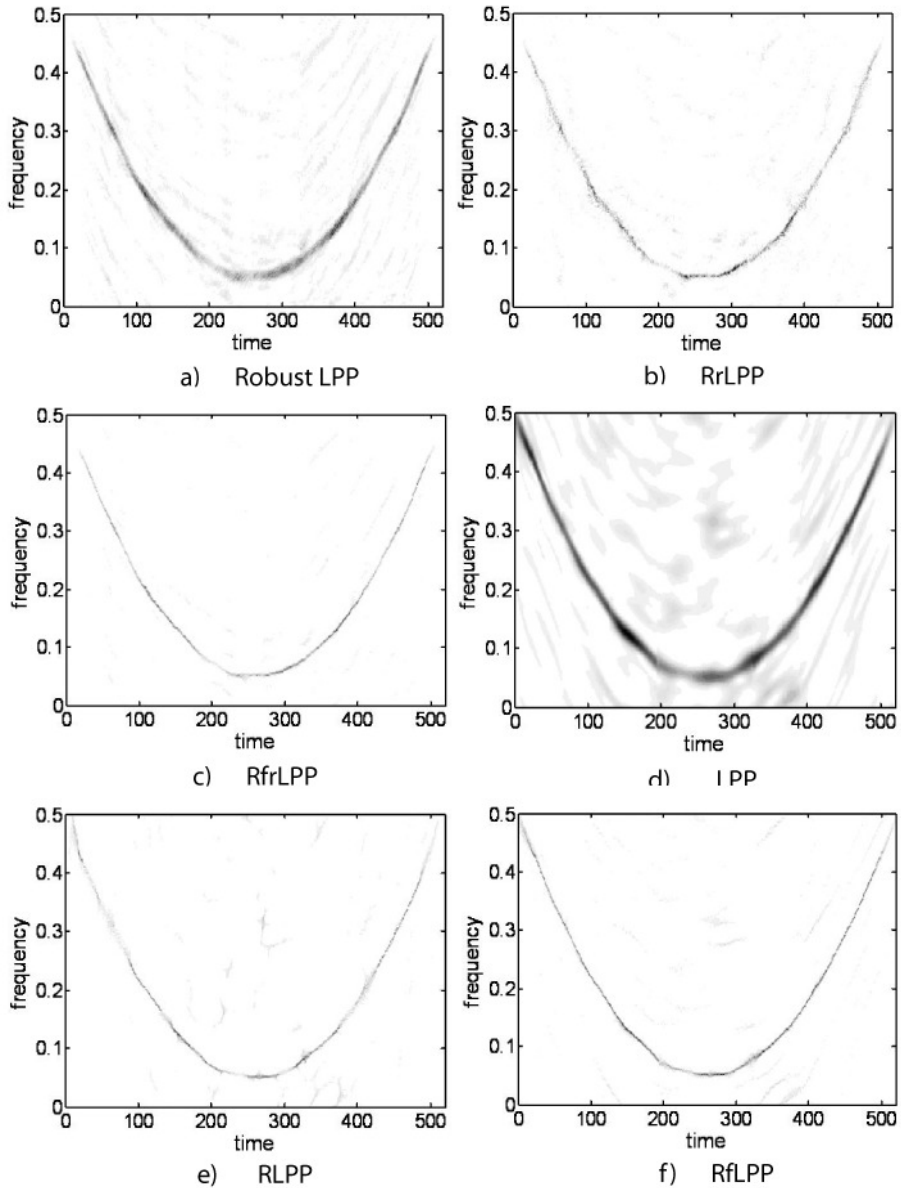

Fig. 10. The LPP-related representations of a signal in AWGN.

respectively, compared with 0.81 and 3.74 seconds for those without any overlap. Therefore, the computational complexity is significantly reduced, i.e., achieving about 47 and 10 times of savings in computation time. In Table I, the computation times for the LPP-related representations are measured on the processing without any overlap between the signal segments, while the computation times for the spectrogram-related representations in Table I are measured on the processing with the maximum overlap to achieve the best possible performance.

In Table I, the computation time needed by the LPP is about 5 times of that needed by the SP. However, it is observed that the robust methods with median filtering, i.e., robust SP and robust LPP, or the reassignment methods,

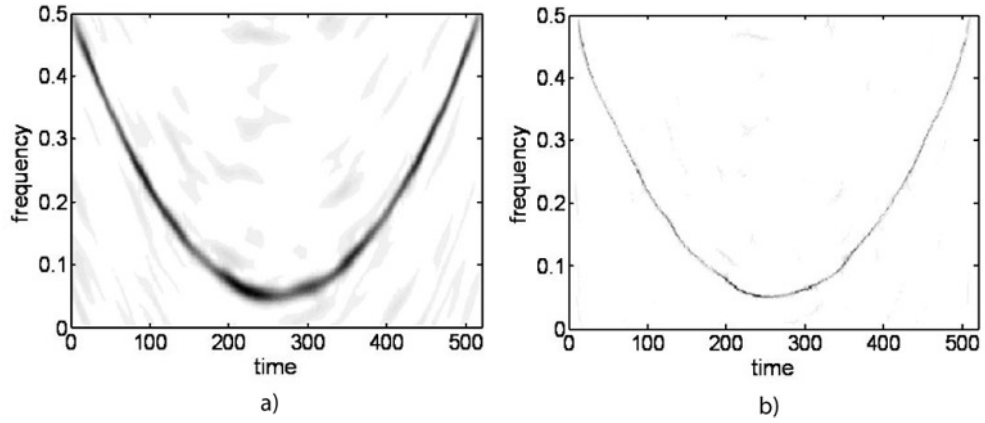

Fig. 11. The LPP and RLPP with the maximum overlap between signal segments.

TABLE I

Comparison on computation time required by various computation methods. The AWGN is $0.75[w_1(t) + jw_2(t)]$ and the impulsive noise is $0.5[w_1^3(t) + jw_2^3(t)]$.

Methods	Computation time (s)
spectrogram	0.1641
reassigned spectrogram	3.8730
robust spectrogram	122.9487
reassigned robust spectrogram	370.3964
LPP	0.8087
reassigned LPP	3.7418
reassigned LPP along the frequency direction	2.9340
robust LPP	123.7826
reassigned robust LPP	364.0574
reassigned robust LPP along the frequency direction	252.0833

i.e., RSP and RLPP, require about the same computation time. It means that as far as the median filtering or reassignment method is involved, the improvements made by the LPPs do not require extra computation time compared with the spectrograms with median filtering or reassignment method. Furthermore, it is also noted that compared to the RLPP and RrLPP, the RfLPP and RfrLPP can reduce the computation times by about 20% and 30%, respectively. It will be shown in the following subsections that the RfLPP and RfrLPP can provide better distribution concentrations and smaller MSEs. Therefore by using these two methods we can achieve significant performance improvements with savings in computation time.

D.3 Distribution concentration

Next we will evaluate the performances in terms of the distribution concentration with the signal $x(t)$ embedded in impulsive noise $n(t) = \alpha[w_1(t)^3 + jw_2(t)^3]$, AWGN $n(t) = w_1(t) + jw_2(t)$, and mixture of these noises $n(t) = \alpha[w_1(t)^3 + jw_2(t)^3] + [w_1(t) + jw_2(t)]$, where $\alpha \in [0, 1.5]$. For each value of SNR or α, measurements of 100 trials are averaged. Similar to the concept of the distribution concentration used in [58], we define the distribution concentration as

$$\mathbf{B} = 10 \log_{10} \frac{E_1}{E_2},$$

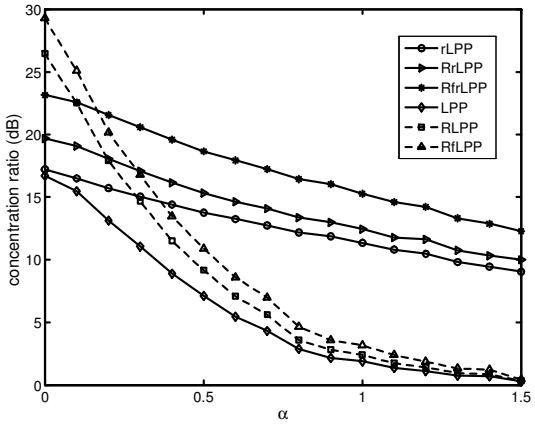

(a) Concentration ratios in impulsive noise

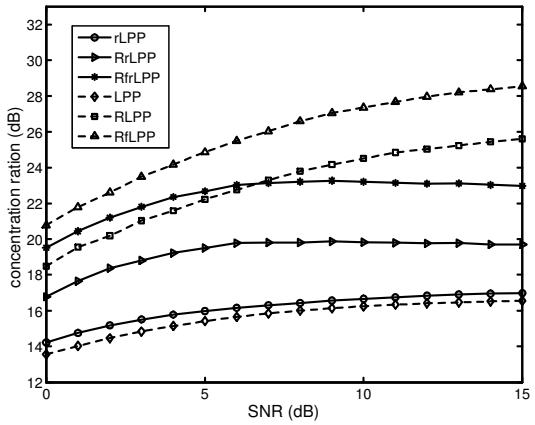

(b) Concentration ratios in AWGN

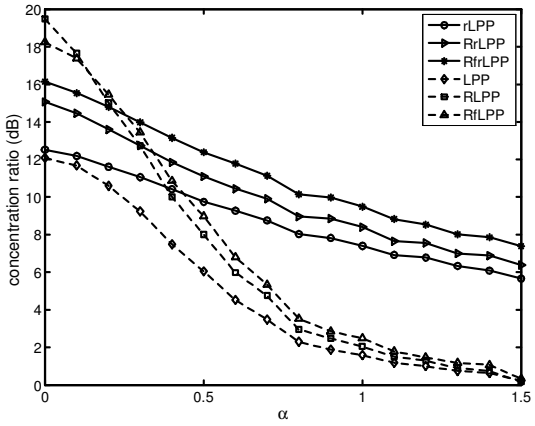

(c) Concentration ratios in mixture noise

Fig. 12. Distribution concentration ratios of various representations in different noise environments.

$$= 10\log_{10}\frac{\text{average}(\text{TFR}(t,\omega)_{(t,\omega)\in R})}{\text{average}(\text{TFR}(t,\omega)_{(t,\omega)\notin R})} \quad (91)$$

where region R corresponds to the IF lines of the signal components, which are determined by the peak values in the TFRs, E_1 is the average energy along the region R, and E_2 is the average energy outside the region R.

For the signal in (90) corrupted by impulsive noise, Figures 12(a) and (b) show that, the robust LPP-related methods with the median filtering are able to improve the distribution concentration. However, the median filtering is not effective to improve the concentration of the signals corrupted by AWGN. In contrast, the reassigned LPP-related methods are effective to improve the concentration for signals in AWGN or impulsive noise. It also confirms that both the median filtering and reassignment operation are necessary to achieve the best distribution concentration for signals in the mixed noise environment, as shown in Fig. 12(c). It is also noted that, the RfrLPP in Fig. 12(a) and the RfLPP in Fig. 12(b) obtain better concentrations, which are consistent with the observations from Figure 8 and Fig. 10, respectively.

D.4 Mean squared errors (MSEs)

We will compare the MSEs of IF estimation achieved by using various LPP-related methods for the signal $S(t)$ embedded in different noise environments. The IF estimation is obtained according to the curve peak positions in the time-frequency transforms, defined as [4]

$$\hat{\omega}(t) = \arg\max_{\omega} \text{TFR}(t,\omega).$$

The MSE of the estimator is defined as

$$\int [\omega(t) - \hat{\omega}(t)]^2 dt,$$

where $\omega(t)$ is the true IF and $\hat{\omega}(t)$ is the estimated IF.

In general, median filtering is useful for minimizing the MSEs when the signal is in impulsive noise environment, as seen in Fig. 13(a) in which larger MSEs are obtained by the LPPs without using median filtering. However, the median filtering has side effects on minimizing

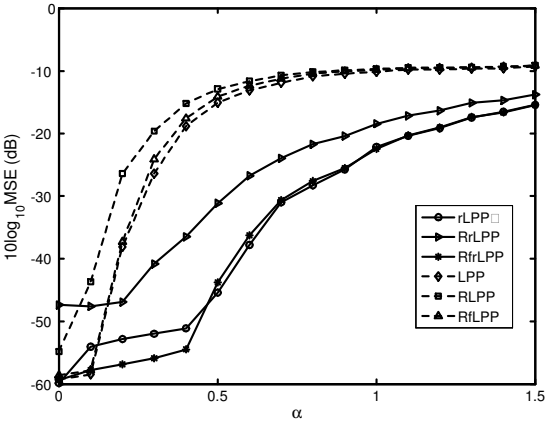

(a) MSE in impulsive noise

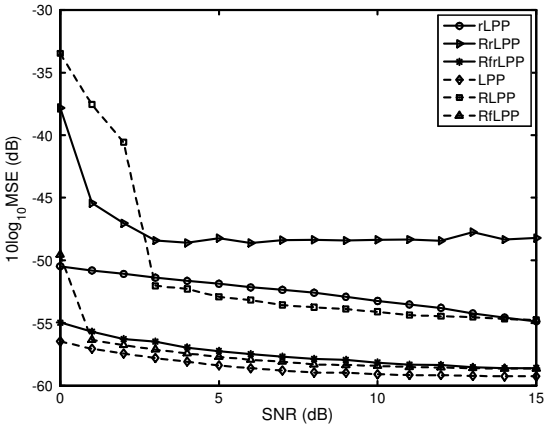

(b) MSE in Gauss noise

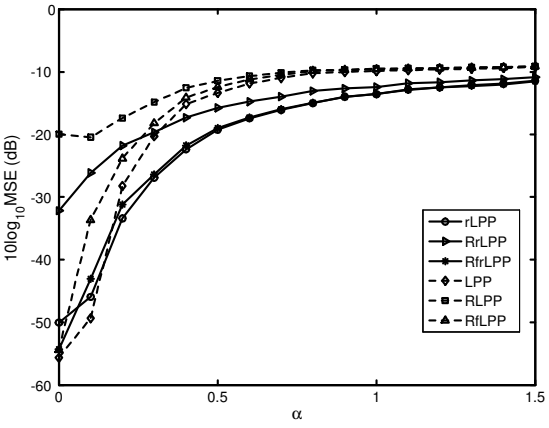

(c) MSE in mixed noise

Fig. 13. MSEs of different representations in impulsive noise, AWGN, and mixed noise.

the MSEs for signals in Gaussian noise environments, which can be seen from Fig. 13(b) that the representations with median filtering achieve larger MSEs than their counterparts. Meanwhile the reassignment operations also have adverse effects on minimizing the MSEs for signals in AWGN or impulsive noise. This can be seen obviously from, for example, Fig. 13(a) and Figure 13(b) that the RrLPP and RLPP achieve much larger MSEs than the robust LPP and LPP, respectively. However, it is interesting to see that in Fig. 13(a), the RfrLPP has almost the same MSEs as the robust LPP, and in Fig. 13(b), the RfLPP has almost the same MSEs as the LPP. It means that the RfLPP and the RfrLPP have little side effects on minimizing the MSEs in AWGN and impulsive noise, respectively.

It should be noted that in this simulation, the testing signal with a parabolic FM law is given as an example. Similar results can be achieved with other kind of frequency modulation law such as the LFM signals and the sinusoidal FM signals.

It is also worth mentioning that in this section the impulsive noise is modelled as $\alpha[w_1^3 + jw_2^3]$. For impulsive noise belongs to Middleton class A model [67], or the standard Cauchy distributed complex noise $v_1(n) + jv_2(n)$ [68], where $v_1(n)$ and $v_2(n)$ are mutually independent with the standard Cauchy distribution $f_v(x) = \dfrac{1}{\pi(1+x^2)}$, similar performance comparisons can also be achieved.

VII. Application examples and potential applications of the LPFT

As presented in Section V, the LPFT can provide higher SNR improvement compared with other transforms such as the STFT and the WVD. Moreover, the LPFT can achieve higher resolution than the STFT and is free from the cross terms that exist in the WVD. The LPFT has been found to be a better tool to deal with signals having time-varying frequencies and has been employed in a variety of practical applications. In ISAR imaging, for example, the LPFT is used to provide more focused images than the STFT [32]. A brief

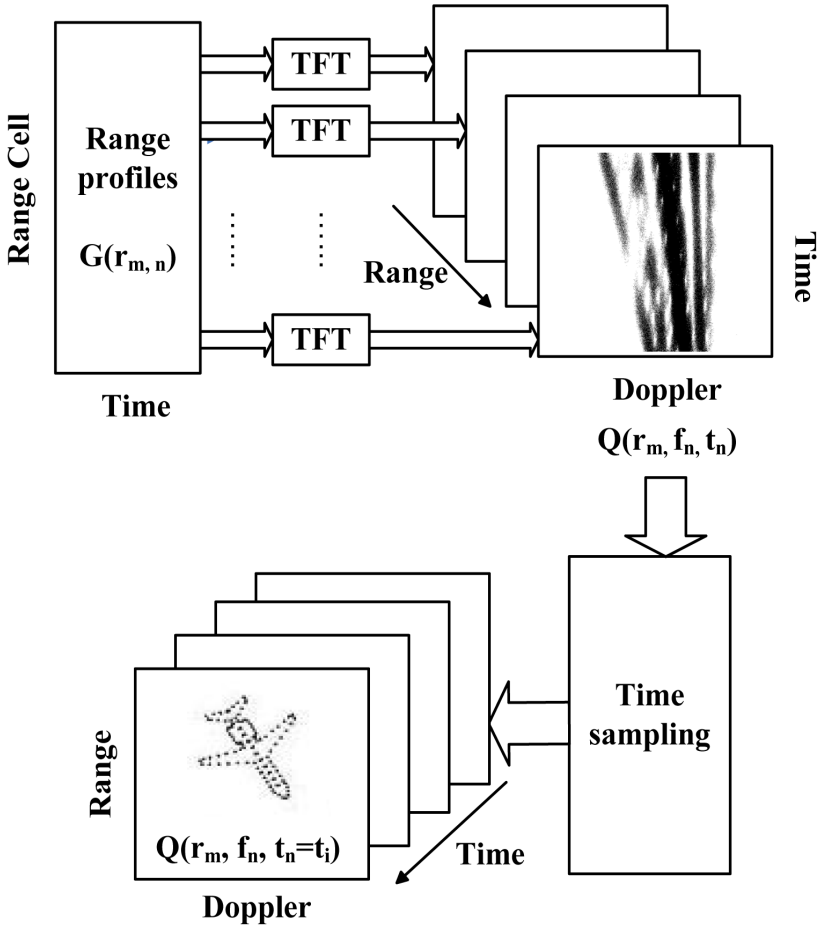

Fig. 14. Illustration of ISAR imaging using time-frequency transform

introduction on this application will be given as follows.

To construct images of radar targets from recorded complex data, radar image formation is often required [6], which is a mapping of a three-dimensional (3D) target onto a two-dimensional (2D) range and cross-range plane. The conventional radar image formation is based on the FT. In ISAR, because the movements of radar targets are usually complicated, motion compensations are generally needed to obtain focused images by using the FT. If the motion compensation is not sufficient, the resulting image can still be blurred when the FT is applied. However, the problem of using the FT can be circumvented if it is replaced by a time-frequency transform (TFT). Various TFTs, such as the STFT [69], the WVD [69] and continuous wavelet transform [70], have been used to mitigate image blurring for improvement on the quality of ISAR images. Because the LPFT is linear, free from the cross terms, and can provide higher resolution for time-varying signal, it is employed as the TFT to obtain higher resolution images, as shown in [32].

To generate the image of the target, the radar transmitter emits a sequence of N pulses and the range resolution is determined by the bandwidth of the pulse. For each transmitted pulse, the total number of range cells, M, is determined by the maximum range covered and the range resolution. The total number of pulses, N, for a given imaging integration

time determines Doppler or cross-range resolution. The radar data sequence is formed as a complex 2D array $G(r_{m,n}), (m = 0, 1, \cdots, M-1; n = 0, 1, \cdots, N-1)$, where M is the number of range cells and N is the number of pulses.

Based on the TFTs, Fig. 14 illustrates the process of radar image formation [6]. Standard motion compensation is needed before the image formation. An $N \times N$ Doppler-time distribution is generated by performing the TFT at each range cell. Then the $M \times N \times N$ range-Doppler-time cube, $Q(r_m, f_n, t_n) = \mathrm{TFT}_n G(r_{m,n})$, is formed by combining the Doppler-time distributions at the M range cells. By time sampling from the cube $Q(r_m, f_n, t_n)$, a range-Doppler image frame $Q(r_m, f_n, t_n = t_i)$ can be obtained for a particular time instant t_i. Each of the N image frames represents a full range-Doppler image with a better resolution at a particular time instant [6]. In contrast, the imaging formation based on Fourier transform generates only one blurred 2D $M \times N$ range-Doppler ISAR image frame from the $M \times N$ radar data set. Therefore, by replacing the Fourier transform with the TFT, a 2D range-Doppler image becomes a 3D time-range-Doppler image cube. By taking time sampling, a temporal sequence of 2D range-Doppler images can be achieved. The time-varying properties of the recorded signals can also be observed from these image frames at various time instants.

The simulation uses the simulated aircraft B727 data [6] with $\mathrm{SNR}_t = -5$dB. The TFT shown in Fig. 14 is replaced by the LPFT. It is assumed that the center frequency of the radar is 9 GHz and the bandwidth is 150 MHz. The total number of pulses used to form the image is 256.

Fig. 15 presents the blurred ISAR image of B727 data constructed by using the FT, and Fig. 16 is the blurred ISAR image constructed by using the STFT. Figure 17 shows the ISAR images formed by using the LPFT. It is observed that the ISAR achieved by using the LPFT is much better than that achieved by using the STFT and the FT since it uses extra parameters to better characterize the IF of the analyzed signals.

Besides the application in ISAR imaging,

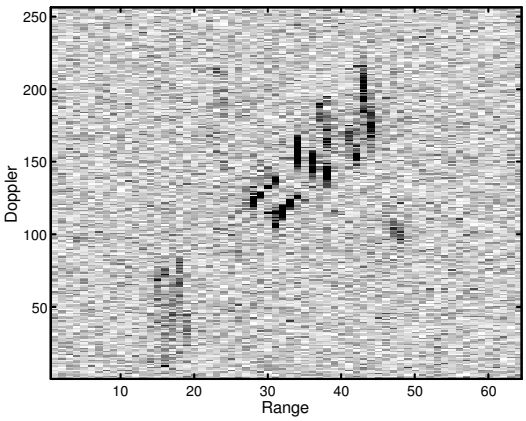

Fig. 15. ISAR image of B727 formed by using the FT

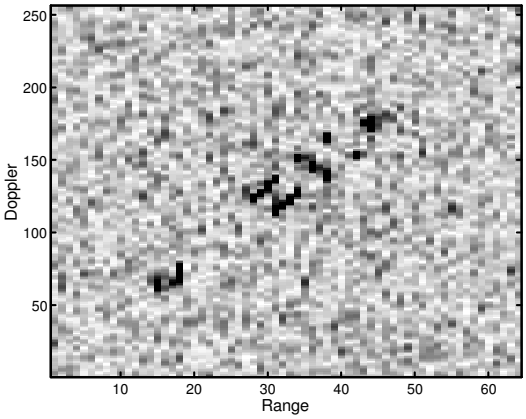

Fig. 16. ISAR image of B727 formed by using the STFT (64th temporal frame)

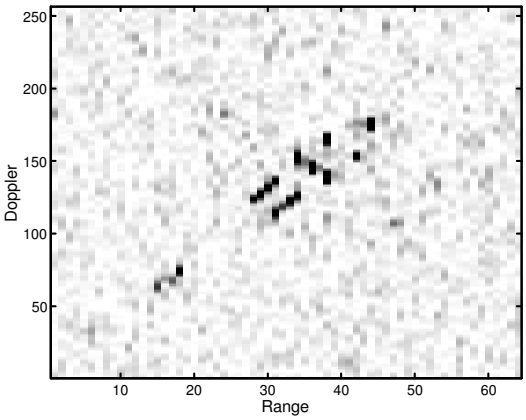

Fig. 17. ISAR image of B727 formed by using the LPFT (64th temporal frame and no overlapping)

the LPFT has also been used in various other applications. The following are some examples.

• In the ISAR, suitable enhancement technique for the fast maneuvering radar targets or targets with fast moving parts is important to achieve improved ISAR images. The LPFT has been used for improvement of the ISAR images in complex reflector geometry cases, as well as in cases fast maneuvering targets [24], [25]. The defocused radar images can be enhanced with a relatively modest calculation burden. Furthermore, the LPFT has been employed for nonstationary interference suppression in noise radar systems [71]. To remove the nonstationary interference, a time-varying filter based on the LPFT is developed and performed in the time-frequency domain by using a binary excision mask.

• The LPFT is used for nonstationary jammer rejection in the spread spectrum communications to improve interference immunity of spread spectrum systems and to provide more reliable signal receiving and decoding performance [26], [27]. Corresponding bit error performance was significantly improved compared with that obtained from the systems based on the STFT.

• In digital video processing, motion estimation is an important topic. By using frame projections on coordinate axis and the $\mu-$propagation [14], the video sequences are mapped to frequency modulated signals. Estimations of the phase coefficients using the LPFT can provide the estimates of velocity and acceleration of moving objects.

• A new form of beamformer based on the LPFT is derived in [72] for source localization and tracking in highly nonstationary environment. This technique can be interpreted as an extension of the conventional beamforming method to nonstationary environment, and it can resolve closely spaced sources provided that their velocities are sufficiently different.

• The LPFT can be used as an estimator of the IF and its derivatives. The technique is based on fitting a local polynomial approximation of the frequency which implements a high-order nonparametric regression. The estimator is shown to be strongly consistent and Gaussian for a polynomial frequency. The corresponding asymptotic covariance matrix and bias of the estimates are studied in [22], [23].

• The concept of the LPFT is also implemented for the polynomial WVD to produce high signal concentration along the IF [28], and it is also extended to the L-Wigner distribution in [73].

Since the LPFT is a generalized form of the STFT, in the areas in which the STFT is used, there exists the potential for generalization and improvement by using the LPFT. The following lists some potential applications of the LPFT.

• To analyze the patterns of time-frequency structures within a musical passage, despite of its low resolution, the STFT is usually employed due to its simplicity. For example, the STFT has been used to analyze the frequency, or pitch, and content of the sounds produced by different musical instruments such as piano, flute and guitar [74]. The STFT has been used for analyzing the rhythmic structure of music and its interaction with melodic structure [75]. Moreover, the STFT has been widely used to process the music signals [76], [77], [78] and the music of bird song [8]. It is obvious that better results can be obtained by using TFRs which can provide higher resolution with reduced or free cross terms, and the LPFT is an appropriate choice.

• The combination of the WVD and Hough transform, that is the Wigner-Hough transform (WHT) has been proposed to detect the LFM signals in noisy environment. However, the WVD has an inherent noise threshold effect problem [79] and therefore cannot give satisfactory representations of the LFM signals in heavy noises. As shown in Section V, the LPFT has a much better noise resistance capability than the WVD and is able to obtain desirable signal representations in the time-frequency domain even in a very low input SNR environment. Therefore, the LPFT can be used for the image formation to detect the chirp signals with very low SNRs, followed by the Hough transform to detect LFM signals. The combination of the LPFT and Hough transform can provide improved performance compared with the WHT especially

when the signals are in heavy noise environment.

- In communications, the adaptive wavelet transform [80], the adaptive STFT [52] and the WVD [81] have been used for the excision of the second-order polynomial phase interference (PPI). All these transforms, except the WVD, do not have optimal concentration property for the second-order PPI, which is the linear chirp interference. However, the undesirable influence of cross terms prevents the WVD from being used for the multicomponent interference excision. As stated in Section VI, when the LPFT is combined with the reassignment method, it can provide perfect localization for chirp signals. Therefore the reassigned LPP can be the proper candidate to excise the second-order PPI in communications.
- To accurately estimate the pitch is important for many speech processing applications, such as speech synthesis, speech enhancement, and speech coding. In common speech pitch estimation methods, the STFT is usually employed with the widely used assumption that the pitch is constant over a segment of short duration [82], [83]. However, this assumption may not apply in reality and leads to inaccurate pitch estimates. Compared with the STFT, the LPFT uses extra parameters to approximate the polynomial phase of the time-varying signals, and therefore it is more suitable to process the time-varying signals such as the speech signals and can achieve better performance for the speech analysis.
- Lamb waves are guided ultrasonic waves that propagate in plates. For ultrasonic nondestructive evaluation methods used to detect and locate flaws in thin plates and to determine their elastic stiffness coefficients, accurate knowledge of the velocity dispersion of Lamb modes is important [84], [85]. Lamb mode dispersion is also essential in the acoustic emission technique for accurately triangulating the location of emissions in thin plates. The time-frequency analysis such as the pseudo WVD and reassigned methods of the spectrogram, the scalogram, the smoothed WVD, and the Hilbert spectrum have been employed to characterize the Lamb mode dispersion [84], [85]. As an appropriate choice to process time-varying signals, the LPFT is hopefully used in the dispersion analysis of Lamb waves.

VIII. Conclusion

In this paper, the local polynomial Fourier transform (LPFT) is reviewed, including its definition, properties, relationships with other transforms such as the STFT, the WVD, the AF and the FrFT. The LPFT for multicomponent signals is presented and discussed. The PTFT and its properties are introduced, and the fast algorithms for the PTFT are also reviewed to achieve better computational efficiency.

To better judge the possibility of detecting the narrowband signals in the frequency domain and the time-varying signal in the time-frequency domain, the definition of the 3dB SNR as in communications is employed for the quantitative SNR analysis of the LPFT. This 3dB SNR definition is transform-domain dependent and directly relates to the bandwidth of the signal. Therefore it is suitable for signals in the time-frequency domain as well as in the time and frequency domains, respectively. Theoretical comparisons on the 3dB SNR performances achieved by using the LPFT, the FT, the STFT and the WVD are presented with simulations to illustrate the advantage of using the LPFT.

The reassignment method is extended to the LPP and the robust LPP to get the reassigned LPP (RLPP) and the reassigned robust LPP (RrLPP), respectively. Performance using various LPP-related methods are compared for signals embedded in additive white Gaussian noise, impulsive noise, and the mixture of additive white Gaussian noise and impulsive noises. Compared with the counterparts without reassignments, the reassigned methods are useful to improve the distribution concentration. However, it is not capable of minimizing the mean squared errors of instantaneous frequency estimation. Furthermore, the reassigned LPP along the frequency direction (RfLPP) and the reassigned robust LPP along the frequency direction (RfrLPP) are preferred because they can achieve good distribution concentrations and small mean square

errors with reduced computational complexities.

Finally, application examples using the LPFT are reviewed and potential applications of the LPFT in the areas such as musical signal processing, interference excision in communications, speech pitch and formant analysis, and dispersion analysis of Lamb waves are discussed to illuminate the future work of the LPFT applications.

References

[1] P. Davis, *Interpolation and Approximations*, Dover, NY, 1975.

[2] D. Wehner, *High-Resolution Radar, Second Edition*, Norwood, MA, 1994.

[3] L. Cohen, *Time-Frequency Analysis*, Prentice Hall, NJ, 1995.

[4] S. Qian and D. Chen, *Joint Time-Frequency Analysis: Methods and Applications*, Prentice Hall, NJ, 1996.

[5] H. Ozaktas, Z. Zalevsky and M. Kutay, *The Fractional Fourier Transform with Applications in Optics and Signal Processing*, Prentice Hall, NY, 2000.

[6] V. Chen and H. Ling, *Time-Frequency Transform for Radar Imaging and Signal Analysis*, Artech House, Boston, MA, 2002.

[7] P. Huber, *Robust Statistics*, John Wiley and Sons Ltd, NY, 1981.

[8] D. Tothenberg, *Why Birds Sing: A Journey into the Mystery of Bird Song*, Basic Books, NY, 2005.

[9] R. Kennedy, *Fading Dispersive Communication Channels*, Wiley, NY, 1960.

[10] B. Boarshash and M. Mesbah, "A time-frequency approach for newborn seizure detection," *IEEE Engineering in Medicine and Biology Magazine*, vol. 20, no. 5, pp. 54-64, 2001.

[11] S. Stanković, I. Djurović, and I. Pitas, "Watermarking in the space/spatial-frequency domain using two-dimensional Radon-Wigner distribution," *IEEE Transactions on Image Processing*, vol. 10, no. 4, pp. 650-658, 2001.

[12] S. Erküçük, S. Krishnan, and M. Zeytinoğlu, "A robust audio watermark representation based on linear chirps," *IEEE Transactions on Multimedia*, vol. 8, no. 5, pp. 925-936, 2006.

[13] I. Djurović and S. Stanković, "Estimation of time-varying velocities of moving objects by time-frequency representations," *IEEE Transactions on Image Processing*, vol. 12, no. 5, pp. 550-562, 2003.

[14] S. Stanković, I. Djurović, and R. Herpers, "Velocity and acceleration estimation in video sequences by the local polynomial periodogram," *International Symposium on Signal Processing and Its Applications (ISSPA)*, vol. 1, pp.145-148, 2003.

[15] A. Orazco-Lugo, M. Lara, D. Mclernon, and H. Muro-Lemus, "Multiple packet reception in wireless ad hoc networks using polynomial phase modulating sequences," *IEEE Transactions on Signal Processing*, vol. 50, no. 5, pp. 1077-1090, 2002.

[16] A. Papandreou-Suppappola and S. Suppappola, "Wideband weyl symbols for dispersive time-varying processing of systems and random signals," *IEEE Transactions on Signal Processing*, vol. 51, no. 8, pp. 2093-2110, 2003.

[17] M. Martone, "A multicarrier system based on the fractional Fourier transform for time-frequency selective channel," *IEEE Transactions on Signal Processing*, vol. 49, no. 6, pp. 1011-1020, 2001.

[18] B. Boashash, "Estimating and interpreting the instantaneous frequency of a signal—Part 2: Algorithms and applications," *Proceedings of the IEEE*, vol. 80, no. 4, pp. 540-568, 1992.

[19] S. Peleg and B. Porat, "Estimation and classification of polynomial-phase signals," *IEEE Transactions on Information Theory*, vol. 37, no. 2, pp. 422-430, 1991.

[20] F. Hlawatsch and G. F. Boudreaux-Bartels, "Linear and quadratic time-frequency signal representations," *IEEE Signal Processing Magazine*, vol. 9, no. 4, pp. 21-67, 1992.

[21] E. Sejdić, I. Djurović, and J. Jiang, "Time-frequency feature representation using energy concentration: An overview of recent advances," *Digital Signal Processing*, vol. 19, no. 1, pp. 153-183, 2009.

[22] V. Katkovnik, "A new form of Fourier transform for time-frequency estimation," *Signal Processing*, vol. 47, no. 2, pp. 187-200, 1995.

[23] V. Katkovnik, "Discrete-time local polynomail approximation of the instantaneous frequency," *IEEE Transactions on Signal Processing*, vol. 46, no. 10, pp. 2626-2637, 1998.

[24] I. Djurović, T. Thayaparan, and L. Stanković, "Adaptive local polynomial Fourier transform in ISAR," *EURASIP Journal on Applied Signal Processing*, vol. 2006, pp. 1-15, 2006.

[25] I. Djurović, T. Thayaparan, and L. Stanković, "SAR imaging of moving targets using polynomial Fourier transform," *IET Signal Processing*, vol. 2, no. 3, pp. 237-246, 2008.

[26] L. Stanković and S. Djukanović, "Order adaptive local polynomial FT based interference rejection in spread spectrum communication systems," *IEEE Transactions on Instrumentation and measurement*, vol. 54, no. 6, pp. 2156-2162, 2005.

[27] S. Djukanović, M. Daković and L. Stanković, "Local polynomial Fourier transform receiver for nonstationary interference excision in DSSS communications," *IEEE Transactions on Signal Processing*, vol. 56, no. 4, pp. 1627-1636, 2008.

[28] L. Stanković, "Local polynomial Wigner distribution," *Signal Processing*, vol. 47, no. 1, pp. 123-128, 1997.

[29] V. Katkovnik, "New method for varying adaptive bandwidth selection," *IEEE Transactions on Signal Processing*, vol. 47, no. 9, pp. 2567-2571, 1999.

[30] V. Katkovnik, "Nonparametric estimation of instantaneous frequency," *IEEE Transactions on Information Theory*, vol. 43, no. 1, pp. 183-189, 1997.

[31] V. Katkovnik, "Local polynomial approximation

of the instantaneous frequency: Asymptotoc accuracy," *Signal Processing*, vol. 52, no. 3, pp. 343-356, 1996.

[32] X. Li, G. Bi, and Y. Ju, "Quantitative SNR analysis for ISAR imaging using LPFT," *IEEE Transactions on Aerospace and Electronic Systems*, vol. 45, no. 3, pp. 1241-1248, 2009.

[33] J. Jeong and W. Williams, "Mechanism of the cross-terms in spectrograms," *IEEE Transactions on Signal Processing*, vol. 40, no. 10, pp. 2608-2613, 1998.

[34] I. Djurović, "Robust adaptive local polynomial Fourier transform," *IEEE Signal Processing Letters*, vol. 11, no. 2, pp. 201-204, 2004.

[35] F. Zhang, Y. Chen, and G. Bi, "Adaptive harmonic fractional Fourier transform," *IEEE Signal Processing Letters*, vol. 6, no. 11, pp. 281-283, 1999.

[36] L. Stanković, "A measure of some time-frequency distributions concentration," *Signal Processing*, vol. 81, no. 3, pp. 621-631, 2001.

[37] S. Barbarossa, A. Scaglione, and G. Giaanakis, "Product high-order ambiguity function for multicomponent polynomial-phase signal modeling," *IEEE Transactions on Signal Processing*, vol. 46, no. 3, pp. 691-708, 1998.

[38] S. Peleg and B. Friedlander, "Multicomponent signal analysis using the polynomial-phase transform," *IEEE Transactions on Aerospace and Electronic Systems*, vol. 32, no. 1, pp. 378-387, 1996.

[39] Y. Wei and G. Bi, "Efficient analysis of time-varying muliticomponent signals with modified LPTFT," *EURASIP Journal on Applied Signal Processing*, vol. 2005, no. 1, pp. 1261-1268, 2005.

[40] M. Ikram, K. Abed-Meraim, and Y. Hua, "Fast qudratic phase transform for estimating the parameters of multicomponent chirp signals," *Digital Signal Processing*, vol. 7, no. 2, pp. 127-135, 1997.

[41] X. Xia, "Discrete chirp-Fourier transform and its applications to chirp rate estimation," *IEEE Transactions on Signal Processing*, vol. 48, no. 11, pp. 3122-3133, 2000.

[42] Y. Wei and G. Bi, "Fast algorithm for polynomial time frequency transform," *Signal Processing*, vol. 87, no. 5, pp. 349-351, 2007.

[43] G. Bi, Y. Ju, and X. Li, "Generalized fast algorithms for the polynomial time-frequency transforms of real-valued sequences," *IEEE Transactions on Signal Processing*, vol. 56, no. 5, pp. 1905-1915, 2008.

[44] G. Bi and Y. Wei, "Fast computation for third-order polynomial time frequency transforms," *Electronics Letters*, vol. 40, no. 5, pp. 789-798, 2004.

[45] G. Bi, Y. Wei, G. Li and C. Wang, "Radix-2 DIF fast algorithms for polynomial time-frequency transforms," *IEEE Transactions on Aerospace and Electronic Syestems*, vol. 42, no. 4, pp. 1540-1546, 2006.

[46] G. Bi and Y. Wei, "Split-radix algorithms for arbitrary order of polynomial time frequency transforms," *IEEE Transactions on Signal Processing*, vol. 55, no. 1, pp. 134-141, 2007.

[47] G. Bi and Y. Ju, "Radix-3 fast algorithms for polynomial time frequency transforms," *Signal Processing*, vol. 88, no. 9, pp. 2316-2322, 2008.

[48] Y. Ju and G. Bi, "Generalized fast algorithms for the polynomial time-frequency transforms," *IEEE Transactions on Signal Processing*, vol. 55, no. 10, pp. 4907-4915, 2007.

[49] X. Xia, "A quantitative analysis of SNR in the short-time Fourier transform domain for multicomponent signals," *IEEE Transactions on Signal Processing*, vol. 46, no. 1, pp. 200-203, 1998.

[50] X. Xia and V. Chen, "A quantitative SNR analysis for the pseudo Wigner-Ville distribution," *IEEE Transactions on Signal Processing*, vol. 47, no. 10, pp. 2891-2894, 1999.

[51] X. Xia, G. Wang, and V. Chen, "Quantitative SNR analysis for ISAR imaging using joint time-frequency analysis−short time Fourier transform," *IEEE Transactions on Aerospace and Electronic Systems*, vol. 38, no. 2, pp. 649-659, 2002.

[52] X. Ouyang and M. Amin, "Short-time Fourier transform receiver for non-stationary interference excision in direct sequence spread spectrum communications," *IEEE Transactions on Signal Processing*, vol. 49, no. 4, pp. 851-863, 2001.

[53] S. Barbarossa and A. Scaglione, "Adaptive time-varying cancellation of wideband interferences in spread-spectrum communications based on time-frequency distributions," *IEEE Transactions on Signal Processing*, vol. 47, no. 4, pp. 957-965, 1999.

[54] L. Stanković, M. Daković, and V. Ivanović, "Performance of spectrogram as IF estimator," *Electronics Letters*, vol. 37, no. 12, pp. 797-799, 2001.

[55] V. Ivanović, M. Daković, and L. Stanković, "Performance of quadratic time-frequency distributions as instantaneous frequency estimators," *IEEE Transactions on Signal Processing*, vol. 51, no. 1, pp. 77-89, 2003.

[56] F. Auger and P. Flandrin, "Improving the readability of time-frequency and time-scale representations by the reassignment method," *IEEE Transactions on Signal Processing*, vol. 43, no. 5, pp. 1068-1089, 1995.

[57] O. Rioul and P. Flandrin, "Time-scale energy distributions: a general class extending wavelet transforms, " *IEEE Transactions on Signal Processing*, vol. SP-40, no. 7, pp. 1746-1757, 1992.

[58] I. Djurovic and LJ. Stankovic, "Time-frequency representation based on the reassigned S-method," *Signal Processing*, vol. 77, no.1, pp. 115-120, 1999.

[59] S. Hainsworth and M. Macleod, "Time frequency reassignment: a review and analysis," *Tech. Rep. CUED/F-INFENG/TR.459, Cambridge University Engineering Department*, 2003.

[60] S. Fulop and K. Fitz, "Algorithms for computing the time-corrected instantaneous frequency (reassigned) spectrogram, with applicaitons," *The Journal of the Acoustical Society of America*, vol. 119, no.1, pp. 360-371, 2006.

[61] X. Li and G. Bi, "The reassigned local polynomial periodogram and its Properties," *Signal Processing*, vol. 89, no. 2, pp. 206-217, 2009.

[62] F. Auger and P. Flandrin, "Generalization of

the reassignment method to all bilinear time-frequency and time-scale representations," *International Conference on Acoustics, Speech, and Signal Processing (ICASSP)*, pp. 317-320, 1994.

[63] I. Djurovic, V. Katkovnik, and LJ. Stankovic, "Median filter based realization of the robust time-frequency distributions, " *Signal Processing*, vol. 81, no. 7, pp. 1771-1776, 2001.

[64] V. Katkovnik, "Robust M-periodogram," *IEEE Transactions on Signal Processing*, vol. 46, no. 7, pp. 3104-3107, 1998.

[65] I. Djurovic and L. Stankovic, "Robust Wigner distribution with application to the instantaneous frequency estimation," *IEEE Transactions on Signal Processing*, vol. 49, no. 12, pp. 2985-2993, 2001.

[66] C. Hoare, "Quicksort," *Computer Journal*, vol. 5, no. 1, pp. 10-16, 1962.

[67] S. Zabin and H. Poor, "Efficient estimation of the class A parameters via the EM algorithm," *IEEE Transactions on Information Theory*, vol. 37, no. 1, pp. 60-72, 1991.

[68] J. Friedmann, H. Messer, and J. Cardoso, "Robust parameter estimation of a deterministic signal in impulsive noise," *IEEE Transactions on Signal Processing*, vol. 48, no. 4, pp. 935-942, 2000.

[69] V. Chen and S. Qian, "Joint time-frequency transform for radar Range-Doppler imaging," *IEEE Transactions on Aerospace and Electronic Systems*, vol. 34, no. 2, pp. 486-499, 1998.

[70] H. Kim and H. Ling, "Wavelet analysis of radar echo from finite-size targets," *IEEE Transactions on Antennas and Propagation*, vol. 41, no. 2, pp. 200-207, 1993.

[71] M. Daković, T. Thayaparan, and S. Djukanović, and L. Stanković, "Time-frequency-based nonstationary interference suppression for noise radar systems," *IET Radar, Sonar and Navigation*, vol. 2, no. 4, pp. 306-314, 2008.

[72] V. Katkovnic and A. Gershman, "A local polynomial approximation based beamforming for source localization and tracking in nonstationary environments," *IEEE Signal Processing Letters*, vol. 7, no. 1, pp. 3-5, 2000.

[73] C. Hory, C. Mellet, J. Valiere, and C. Depollier, "Local polynomial time-frequency transform formulation of the pseudo L-Wigner distribution," *Signal Processing*, vol. 81, no. 1, pp. 233-237, 2001.

[74] J. Alm and J. Walker, "Time-frequency analysis of musical instruments," *SIAM Review*, vol. 44, no. 3, pp. 457-476, 2002.

[75] X. Cheng, and J. Hart, and J. Walker, "Time-frequency analysis of musical rhythm," *Notices of the American Mathematical Society*, vol. 56, no. 3, pp. 356-372, 2009.

[76] G. Don and J. Walker, "Music: A time-frequency approach," [Online] Available at: www.uwec.edu/walkerjs/media/TFAM.pdf.

[77] M. Dorfler, "Time-frequency analysis for music signals: A mathematical approach," *Journal of New Music Research*, vol. 30, no. 1, pp. 3-12, 2001.

[78] J. Walker and A. Potts, "Time-frequency spectra of music," [Online] Available at: www.uwec.edu/walkerjs/media/TFSM.pdf.

[79] P. Rao and R. Taylor, "Estimation of instananeous frequency using the discrete Wigner distribution," *Electronics Letters*, vol. 26, no. 4, pp. 246-248, 1998.

[80] M. Tazebay and A. Akansu, "Adaptive subband transforms in time-frequency excisers for DSSS communications systems," *IEEE Transactions on Signal Processing*, vol. 43, no. 11, pp. 2776-2782, 1995.

[81] S. Lach, M. Amin, and A. Lindsey, "Broadband interference excision for software-radio spread-spectrum commnications using time-frequency distribution synthesis," *IEEE Journal on Selected Areas in Communications* , vol. 17, no. 4, pp. 704-714, 1999.

[82] R. Mcaulay and T. Quatieri, "Pitch estimation and voicing detection based on a sinusoidal speech modal," *International Conference on Acoustics, Speech, and Signal Processing (ICASSP)*, pp. 249-252, 1990.

[83] B. Resch, M. Nilsson, A. Ekman and W. Kleijn, "Estimation of the instantaneous pitch of speech," *IEEE Transactions on Audio, Speech, and Language Processing*, vol. 15, no. 3, pp. 813-822, 2007.

[84] J. Qu and J. Jarzynski, "Time-frequency representations of Lamb waves," *Journal of the Acoustical Society of America*, vol. 109, no. 5, pp. 2669-2676, 1999.

[85] W. Prosser, M. Seale, and B. Smith, "Time-frequency analysis of the dispersion of Lamb modes," *Journal of the Acoustical Society of America*, vol. 105, no. 5, pp. 1841-1857, 2001.

[86] G. Bi, et al., LFM signal detection using LPP-Hough transform, *Signal Process*, 2010.